CHARACTERIZATION OF MICRO-TEXTURED CUTTING TOOL SURFACES FOR MACHINING APPLICATIONS

by

KAUSHALENDRA PATEL

A thesis submitted to the

School of Graduate Studies

Rutgers, The State University of New Jersey

In partial fulfillment of the requirements

For the degree of

Master of Science

Graduate Program in Industrial and Systems Engineering

Written under the direction of

Dr. TUĞRUL ÖZEL

And approved by

_____

_____

_____

_____

New Brunswick, New Jersey

May 2019

ABSTRACT OF THE THESIS

Characterization of micro-textured cutting tool surfaces for machining applications

by KAUSHALENDRA PATEL

Thesis Director:
Dr. Tuğrul Özel

For high productivity, sustainable cutting tools with longer tool life and higher durability, which can withstand high temperature and pressure rises during high cutting speeds, are required in difficult-to-cut machining operations in aerospace, automotive, naval, nuclear and other industries. Currently, cutting coolants and lubricants (lubricoolants) are widely used in industry for thermal and tribological management which provide negative impacts on sustainable environment. The use of lubricoolants has to be reduced or totally eliminated through dry machining, decreasing the environmental hazard and manufacturing cost for improved sustainability. Micro-textured cutting tools can play an important role to achieve this goal. There are several distinct advantages offered by micro-textures applied to cutting tool surfaces to reduce cutting forces, friction, wear and material adherence. However, it is not clear what the optimum pattern and dimensions of

these micro-micro-textures should be to obtain minimum forces and wear when using textured cutting tool surfaces in machining processes.

The current work is aimed at investigating the effect of micro-textured insert designs on the cutting forces, but also the effect of micro-groove dimension on the tool wear with experiments. It was expected that the proposed cutting tool surfaces will improve the tribological performance at tool and workpiece interfaces and reduce cutting forces, stresses, and temperatures, and consequently lower usage of energy, coolants, and lubricants in machining of difficult-to-cut materials.

In this research, we investigated the effect of various micro-textured insert designs on the cutting forces and tool wear with experiments in machining titanium alloy Ti-6Al-4V and alloy steel 4340. It was found that micro-texture parameters affect cutting forces and tool wear. Cutting forces are measured by using force dynamometers and the surface topography of the micro-textured tool surfaces were inspected using optical microscopy and focus variation techniques. Micro-texture parameters, groove depth, width, and spacing, are found to be influential on the amount of material smearing into grooves and adhering on the tool surface while reducing thrust forces due to lower contact. Multi-objective optimization studies were conducted to find cutting conditions and micro-groove parameters in machining steel alloy 4340 that minimizes cutting forces and wear. Therefore, the micro-texture design on the tool surfaces can be optimized to obtain lowered cutting forces, improved tool wear, and minimal material adherence. Micro-textured cutting tool parameters as decision variables can be optimized using appropriate optimization strategy that can be obtained from the solution sets. These micro-textures will enable users to practice environmentally sustainable machining through a better application of modern methods such as minimum quantity lubrication, near- dry cutting, cryogenic machining, and solid lubricants.

ACKNOWLEDGMENTS

First, I would like to express my deepest gratitude towards the person who inspired me and helped me on each and every step to make this possible, my M.S. thesis advisor, Dr. Tuğrul Özel. Without his endless support, guidance and motivation this study would not have become possible. I am grateful to him for his constant encouragement and belief in my work during whole master's coursework.

I am thankful to my MS thesis committee members, Dr. Myong K. Jeong and Dr. James T. Luxhøj for the suggestions and constructive advice I received from them. I would also like to thank Dr. Melike-Baykal Gursoy who served as ISE graduate director at Rutgers, for all their support.

The Rutgers University Industrial and Systems Engineering Department for allowing me to use their facility and resources to complete this study. Mr. Brian Alden, Design Specialist who helped whenever technical support needed. The administrators of ISE department at Rutgers, Ms. Cindy Ielmini, Ms. Barthi Ponnuraj and Ms. Laura Kasica.

I appreciate all the help from my colleagues, Mr. Suril Shah, Mr. Guoliang Liu and Mr. Jixiong Fei. Their help and technical support were significant for me to get good reference on different parts of this research work.

Finally, I want to thank my parents, brother and grandmother for having faith in me and their constant support and motivation. I will always remember their sacrifices.

DEDICATION

To my parents, God and Gurus.

For their constant blessings, support and love from long distance.

TABLE OF CONTENTS

LIST OF FIGURES

LIST OF TABLES

LIST OF SYMBOLS

μ	Friction coefficient [-]
w_c	Width of cut [mm]
w	Width of micro-groove [μm]
l	Length of micro-groove [μm]
s	Spacing of micro-groove [μm]
d	Depth of micro-groove [μm]
t	Distance of micro-groove from cutting edge [μm]
a_p	Axial depth of cut [μm]
f	Feed rate [mm/rev]
F_c	Cutting force [N]
F_t	Thrust force [N]
F_f	Feed force [N]
t_c	Chip thickness [mm]
$T_{cutting}$	Cutting time [s]
v	Cutting velocity [m/min]
α	Clearance angle [°]
σ	Normal stress [N/mm^2]
τ	Shear stress [N/mm^2]
r_ε	Nose radius [μm]
r_β	Cutting edge radius [μm]
T_0	Ambient temperature [°C]
Tm	Melting temperature of the material [°C]
l_{smearing}	Chip smearing length [mm]
l_{severe}	Severe wear length [mm]
l_{sliding}	Sliding wear length [mm]

CHAPTER 1

INTRODUCTION

1.1 Introduction and Definitions

In today's global market conditions, sustainable cutting tools with longer tool life and higher durability which can withstand high temperature and pressure rises during high cutting speeds (>100 m/min) are required in modern material removal process (Fratila 2010; Jawahir et al., 2016). Industry broadly uses cutting coolants, various types of lubricants including minimum quantity lubrication systems, and cryogenic systems for thermal and tribological management of metal cutting processes which certainly add significant cost, negatively impacts environment, and are detrimental to sustainability of resources (Bouzakis et al., 2012; Helu et al., 2012).

Currently, cutting coolants and lubricants are widely used in industry for thermal and tribological management which provide negative impacts on sustainable environment and ineffectiveness due to additional cost involved acquiring and disposing of them (Haapala et al., 2013). The use of coolant and lubricants must be reduced or eliminated in metal removal processes, decreasing the environmental hazard and manufacturing cost for improved sustainability (Arrazola et al., 2013; Filipovic & Stephenson 2006; Haapala et al., 2013). In order to enhance cutting tool performance, coatings with high hot hardness, superior thermal and frictional properties ought to be employed.

It is the motivation of this proposed thesis that the use of such chemicals, auxiliary thermal and tribological management systems to be reduced or eliminated in advanced machining processes for coolant-free/ lubricant-free machining and improved sustainability.

Micro-textured surfaces had been reported to improve the tribological performance between parts in contact, by changing the normal stresses distribution, improving the friction coefficient, and reducing the amount of heat transferred between the parts (Nakano et al., 2007; Ramesha et al., 2013). In machining applications, these reduced normal stresses and temperature contribute to improved wear resistance and machining performance, and to eliminate the need to lubricants or coolants during the machining performance (Arslan et al., 2016; Sharma & Pandey 2016).

Traditionally, flood of liquid cutting fluid is directed over cutting action area to reduce heat and friction. But, over the time liquid cutting fluid has raised concerns about health issues, negative impacts on environmental, and increased cost. Therefore, to reduce the use of lubricants, researchers have investigated dry machining (Klocke et al., 1997), near-dry machining (NDM) or minimum quantity lubrication (MQL) machining (Weinert et al., 2004), and cryogenic machining. It has been proposed that the surface structures might contribute to improving the cutting performance by reducing the contact area, retaining the lubricant or debris of the process and promoting a lubricant film in the interface tool-workpiece (Kawasegi et al., 2009). However, cutting tool materials (e.g. tungsten carbide, ceramics, cubic boron nitride and polycrystalline diamond) are difficult to be machined for texturing by using mechanical force because of high material hardness and complex geometries. For this reason, a large amount of studies has been carried out to structure cutting tools and texturing using laser technology, electrical discharge machining, electro-chemical machining, micro grinding, and ultrasonic machining techniques. Structuring of cutting tools has significant potential impact for tools that operate under demanding heat and friction conditions.

In the cutting tools, the structured surface consisting of grooves oriented perpendicular (at 90º) to the cutting edge has promoted a reduction in cutting forces, reduced wear on the rake face and enhanced tool life (Sharma & Pandey 2016). Moreover, a couple of studies have also found a reduction in flank wear by using structures to modify the flank surface. Pattern of texture and its

characteristics such as depth, spacing, length, distance from cutting edge, and orientations, etc. also effect the performance. These textures can be used as reservoir of solid lubricants. Use of solid lubricants such as Boric acid, calcium fluoride, molybdenum disulphide, and graphite, etc. can provide excellent lubrication during cutting operation. With reduced chip contact area due to textures and lubrication effect provided by the solid lubricants, cutting performance of the tool is greatly elevated (Deng et al., 2012).

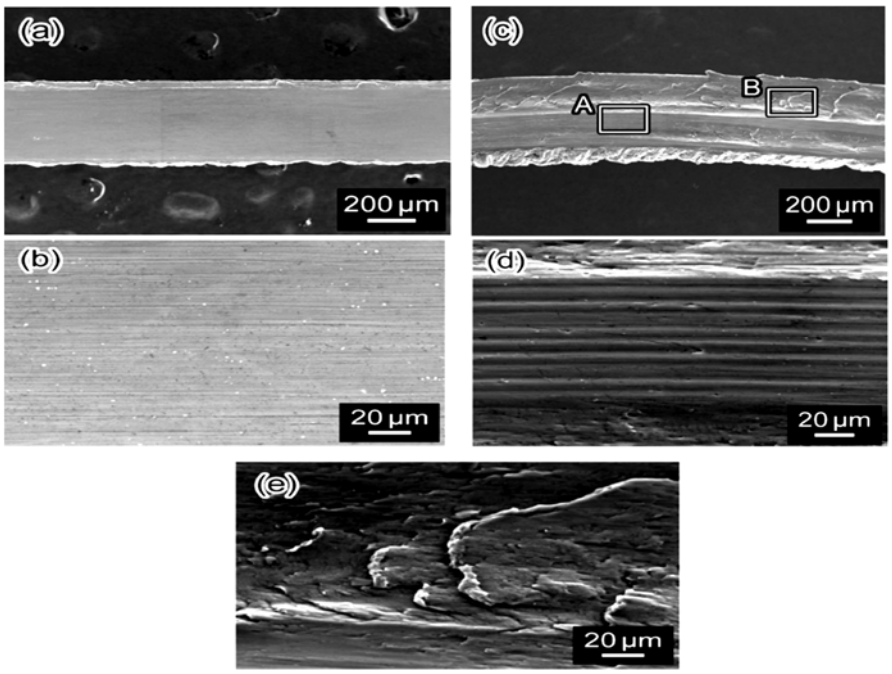

Figure 1.1 SEM Images of chips generated by (a,b) nano textured perpendicular grooves; (c,d,e) nano textured parallel grooves marks (Kawasegi et al., 2009).

1.2 Significance of Surface Texturing and Structuring

Texture is an inherent attribute of any surface encompassing roughness, waviness and lay (ASME 2009). In Evans and Bryan (1999), three definitions were elaborated for structured surfaces, engineered surface and texture as follows. Structured surfaces are surfaces with a deterministic pattern of usually high aspect ratio geometric features designed to give a specific function. Engineered surfaces are surfaces where the manufacturing process is optimized to generate variation

in geometry and/or near surface material properties to give a specific function. Texture (and the associated verbs) is restricted to its current standardized meaning of roughness, waviness, and lay.

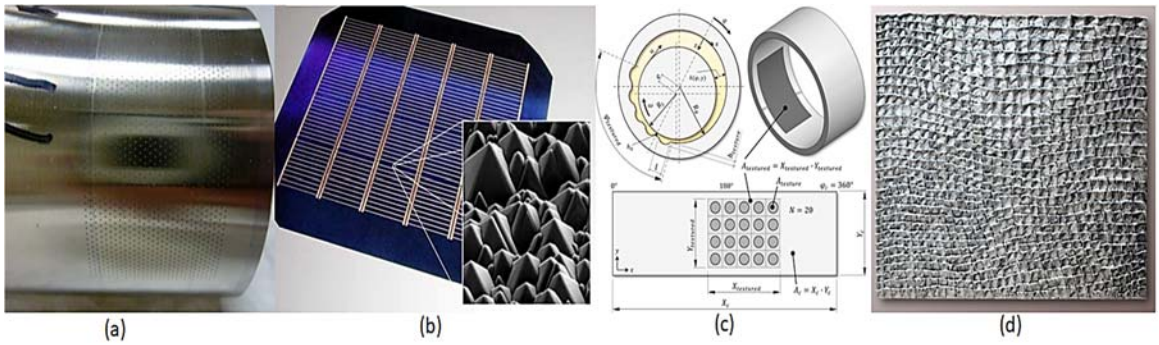

Figure 1.2 (a) Image of laser dimpled implant surface (b) nano textured solar panels (c) nano textured journal bearings (d) surface textured wall art

Surface texturing is being used in variety of fields such as bioengineering to improve biocompatibility of metal implant surfaces (Pou et al., 2017), electronics to improve efficiencies of silicon wafer, automobile to reduce friction in moving mechanical components i.e. pistons, bearings, camshaft etc., cutting tools to reduce friction and improve lubricity, etc. (Sharma & Pandey 2016), arts for specific applications.

1.3 Benefits of Structured Tool Surfaces in Machining Processes

In the 1960s emerged some proposals of surface modification in cutting tools by creating chip breakers and modifying the contact length between the chip and tool (Nakayama 1961). However, these developments did not suggest the creation of structured surfaces on cutting tools. In 2006 a paper was published applying structured surfaces and analysing the effects in a cutting process (Enomoto et al., 2006), This was followed by work on tools and milling processes (Enomoto et al., 2007; Sugihara, Enomoto 2009; Enomoto, Sugihara 2010; Chang et al., 2011; Enomoto et al., 2012, Sugihara, Enomoto 2013). Subsequently, various authors covered the turning process (Jianxin et al., 2009; Lei et al., 2009; Kawasegi et al., 2009; Obikawa et al., 2011; Wenlong et al., 2011; Koshy, Tovey 2011; Jianxin et

al., 2012; Xing et al., 2014) and the drilling process (Kawasegi et al., 2010a; Kawasegi et al., 2010b; Ling et al., 2013). Texture geometry can hold some solid lubricants inside it. Jianxin et al. (2012) discussed about cutting tools deposited with WS_2 solid lubricant in textured surface and found it supportive. The influence of micro-textures on cutting tool surfaces has been investigated for machining different materials in the literature.

Arslan et al. (2016) presents a critical review on the surface texturing to improve tribological properties of cutting tools with a broad range of applications in machining processes. In the milling operation, Enomoto et al. (2012) found that groove depth and direction effect the cutting performance and increase wear resistant. Same researchers also found that small spacing and small width of groove spreads lubricants evenly on cutting surface.

1.4 Motivation and Research Objectives

The main motivation for this thesis is to achieve higher sustainability of metal cutting processes in terms of reduced friction, improved wear-resistance and eliminated coolant usage by developing micro-textures for advanced cutting tools and implementing them in high speed machining for advanced metal alloys such as alloy steels and titanium alloys.

For achieving higher tool performance, new knowledge on the micro-texturing of tool surfaces and multi-functional coatings must be generated. The main focus of this research is to test the hypothesis of micro-textured cutting tool surfaces can successfully be created for not only improving friction characteristics and wear resistance of the tool surfaces, but to also effectively form superior tool surfaces for applications in high speed machining of difficult-to-cut materials that would potentially minimize consumption of environmentally harmful lubricants and coolants (lubricoolant), hence enable sustainable machining of advanced end products. The expected results should highly advance industry about the optimum understanding of lubricoolant usage in machining of difficult-to-cut metal alloys where dry machining is not always practical.

This thesis research will seek answers to the following questions. How can one understand how the textured tool performs during dry cutting process? How would textured and coated tools perform? What are the effects on thrust and cutting forces due to texture? How does adding micro-texture contribute to the frictional behaviour? What is the optimum micro-texture design? How does texture effect the tool wear and tool life?

CHAPTER 2

SURFACE TEXTURING AND STRUCTURING

This chapter provides a review of surface modification techniques not only for modifying the structure of cutting tool surfaces but also for applying specially design textured geometries to improve the surface performance. As we know due to high strength, cutting tool materials (e.g. tungsten carbide, ceramics, cubic boron nitride and polycrystalline diamond) are difficult to be machined. But recent advanced manufacturing technologies have made it possible to work with all these hard materials proficiently. Generally, none conventional machining techniques are used for this purpose. The various techniques of surface texturing can be divided into the following categories: (i) melting and vaporization such as electric discharge machining (EDM); (ii) ablation such as laser surface texturing; (iii) forced material removal such as micro-grinding, sand blasting, abrasive jet machining (AJM), ultrasonic machining (USM), and vibro-mechanical texturing; (iv) dissolution such as chemical etching and electro-chemical machining (ECM); and (v) material addition such as physical vapor deposition (PVD) and chemical vapor deposition (CVD).

2.1 Review of Surface Texturing and Structuring

According to the literature, there are four main designs for the micro-textures on cutting tools: a) micro-grooves perpendicular to the cutting edge, b) micro-grooves parallel to the cutting edge, c) micro-grooves diagonal to cutting edge at an angel, d) dimpled cutting surface tools, and e) cross patterned grooves on the cutting surface (Fig. 2.1 and Fig. 2.2).

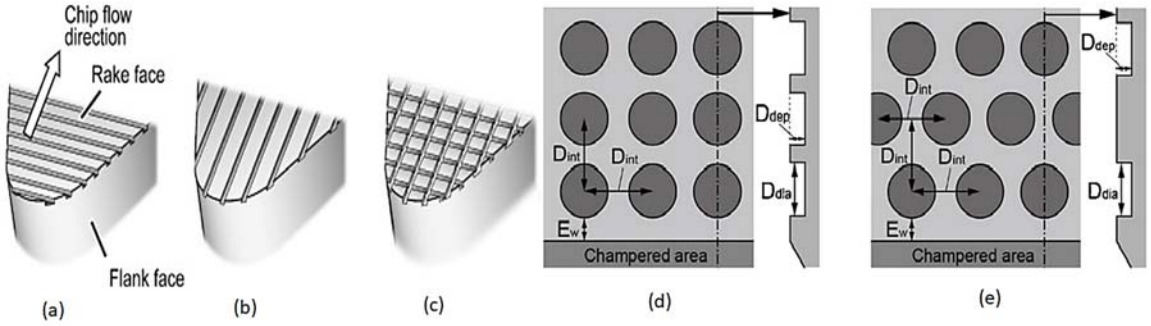

Figure 2.1 Direction of the texture (a) perpendicular and (b) parallel to the chip flow direction. (c) Cross-patterned texture (Kawasegi et al., 2009). Laser dimpled textures patterns (d-e) (Sugihara et al., 2017).

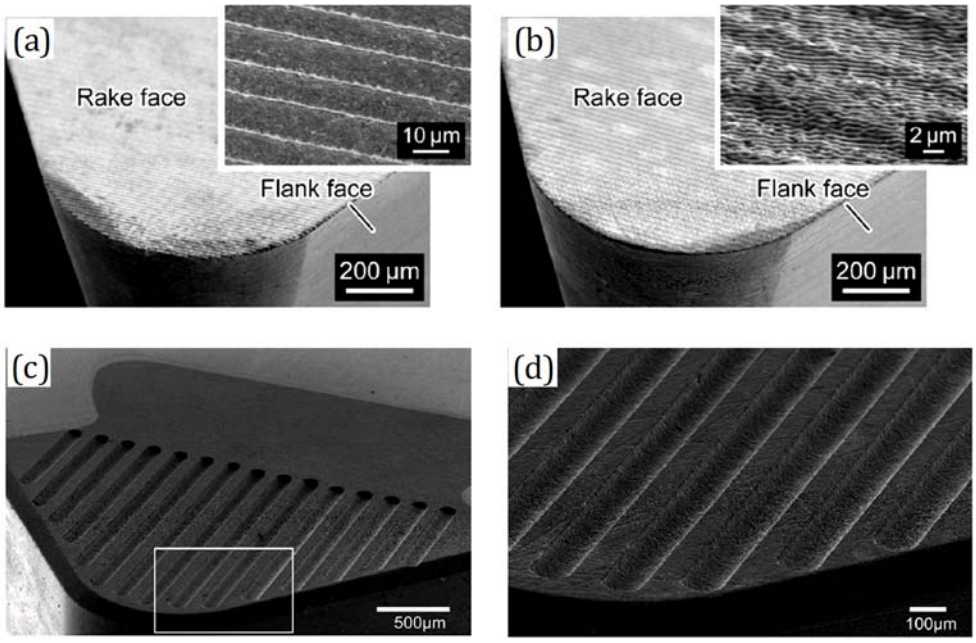

Figure 2.2 Images of micro-textured (10µm spacing) and nano-textured (800 nm spacing) carbide tool rake faces by using femtosecond laser micro-machining (a-b) (Kawasegi et al., 2009), diagonal micro-grooves on cBN tool rake surface by using micro-EDM milling (c-d) (Kim et al., 2016).

The benefits of using textured tools for cutting purposes have been demonstrated in several studies conducted over the past few years. These benefits include a reduction in the coefficient of friction, a reduction in the adhesion of a material, and a reduction in cutting forces by minimized friction at the tool-chip interface and smooth chip removal (Kawasegi et al., 2009).The effect of the decrease in friction due to the texture strongly depends on the shape of the texture, and significantly lower friction can be achieved when the scale of the texture is on the order of micrometres or nanometres rather than submillimetre (Kawasegi et al., 2009). Koshy et al. (2011) investigated the reduction in feed and cutting forces with textured tool (Fig. 2.3). They also investigated the effect of micro-texture location from the cutting edge using perpendicular grooved tools in machining steels. Their findings revealed that the friction angle is minimal when the beginning of texture is 2-3 times of the feed value per revolution.

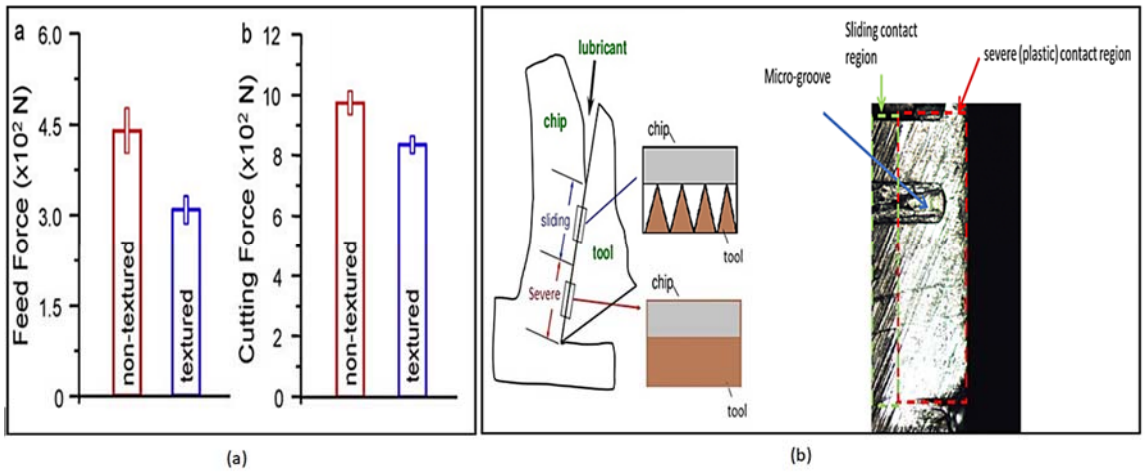

Figure 2.3 (a) Effect of texturing on forces in continuous cutting of steel (Koshy et al., 2011) (b) Effect of texturing on friction in continuous cutting of steel.

The effects of parallel texture parameters (depth, width, spacing, and distance from tool cutting edge) on cutting forces and friction were also investigated by Yang et al. (2014) where cemented carbide tools were used in dry and cryogenic cutting of titanium alloy Ti-6Al-4V. Dimple-texture results in the beneficial influence on tribological properties (Wang Yan-Ging et al., 2009). Micro dimples on the rake face of a cutting tool effectively suppress the crater wear in cutting medium carbon

steels, and the effect can be obtained even under dry cutting conditions (Sugihara et al., 2017).

2.2 Abrasive Finishing and Grinding Based Grooving

Abrasive materials and grinding wheels are used for grinding and fine polishing of metal surfaces. Diamond, cubic boron nitride, aluminum oxide, silicon carbide, and ceramic grains, etc. grains are used to make these wheels. Micro-grinding is a simple and inexpensive process used to create micro surface modifications. Grinding has been used widely for grooves with small dimensions. The reason behind this is micro-grains are used for grinding cutting of only a small amount of material. Still, it is not always superior among other methods. Various problems are encountered while forming the accurate grinding tool shapes, because the grain size must be taken into consideration when the grinding tool size is very small.

Diamond is the hardest material among all the materials which are used for grinding purpose. Diamond grinding wheels are made from polycrystalline diamond and bond metal. Dressing of diamond wheel is performed first in order to give the tip of the wheel our chosen shape. Xie et al. (2012) used diamond wheel to precisely fabricate micron-scale grooves. The diamond wheel tip is first sharpened using CNC mutual wear truing; then the trued diamond wheel tip is patterned on tool rake surface through a traverse grinding with micron-scale depth of cut. Along with the mutual wear of grinding wheel and GC dresser, the grinding wheel section profile is gradually formed to be a stable wheel V-tip shape no matter what shapes the grinding wheel and the GC dresser initially are.

In order to assure the integrity of ground micro-grooves, rough grinding and fine grinding are in succession performed by controlling the depth of cut. The aspect ratio of the tool must be very low. Therefore, deep narrow cavities cannot be obtained by using micro-grinding.

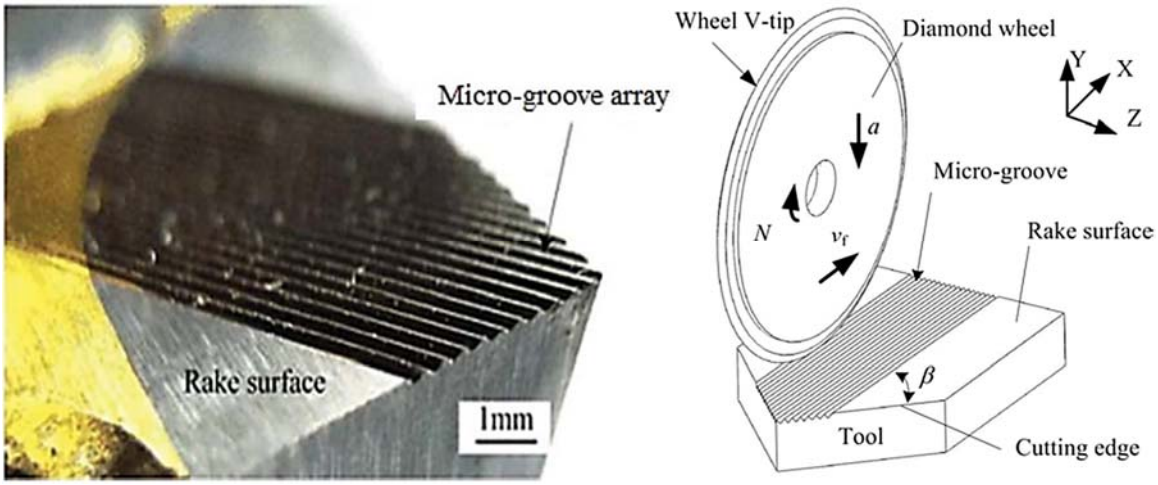

Figure 2.4 (Left) Micro-grooved tool created by micro grinding process (Right) Micro-grinding of micro-groove array on tool rake surface (Xie et al., 2012)

2.3 Micro Electric Discharge Machining Based Grooving

Electric discharge machining (EDM) is a thermal material removal process. Electrical discharges between the tool electrode and the workpiece remove material. The higher frequency of the electrical charges causes melting and vaporization of material on both, electrodes and workpiece material. Material removal rate is high for workpiece material then the electrode. A non-conducting fluid (dielectric fluid) is used to enhance the material removal process. Dielectric fluid is present in the working gap between the tool and the workpiece. The voltage applied during machining depends on the working gap and dielectric fluid conductivity.

The dielectric fluid has several functions. It isolates the tool electrode from the workpiece electrode, thus enhancing current density in the plasma channel. It also cools the heated electrodes and removes the particles after the discharge during the flushing process, thus preventing a short circuit due to developing particle.

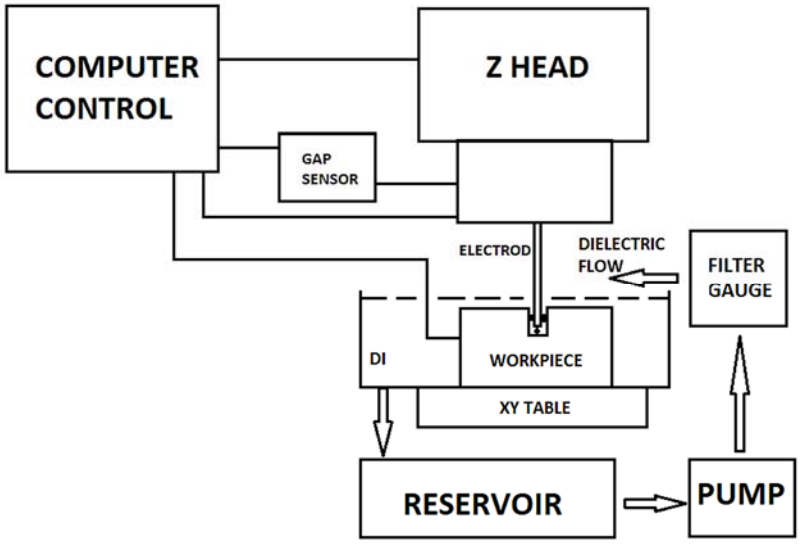

Figure 2.5 Schematic diagram for micro-EDM milling.

Micro-EDM is an application of electric discharge machining on micro scale. It has been developed to make micro size textures and structures. Micro-EDM requires micro-scale electrodes and electric energy lower than 100 *mJ* per discharge. There are various types of micro-EDM, including die-sinking micro-EDM, micro-wire EDM, micro-electric discharge drilling, and micro-electric discharge.

To achieve a high-quality surface, EDM machining is done in several steps. Utilizing EDM for texture creation offers important advantages, such as smaller feature dimensions, lower machining forces, complex geometrical structures, smoother surfaces, absence of mechanical stress on the workpiece, greater precision, and a wider choice of tool material compared to mechanical processes. EDM has some limitations such as low material removal rate, poor surface, heat-affected zones on the surface, and the inability to ensure that the workpiece dimensions.

2.4 Micro Electrochemical Machining Based Grooving

In the electrochemical machining (ECM) process, material is removed through anodic dissolution via the electrolysis process. The machining shape of ECM is determined by the shape of the electrode or design of masking on surface. ECM

has some extraordinary benefits. The machined surface of ECM is very smooth, and machining does not affect any layer. This characteristic of ECM makes it suitable for smoothing of micro-metallic products. To adjust suitable amount of micro-material removal, low current and short pulse are required. The use of high-resistance electrolytes can also produce a low current. Fig. 2.6 shows Schematic diagram of electrochemical machining.

An electrolyte jet has been used in place of metal as a micro-tool. Electrochemical dissolution can be localized by using a high-speed jet. This enables the machining of micro-indentations with controlled dimensions by switching the current synchronously to the movement of the workpiece. Micro-grooves with submicron width can be obtained by using the scanning tunneling microscope (STM) technique with ECM, since removal of material in ECM is essentially an atom by atom process.

Due to its low production cost, high efficiency, absence of a heat-affected layer, and lack of tool wear, ECM is more advantageous than other texture machining techniques. ECM can create surface textures through mask-less or removal of through-mask material. Through-mask ECM is more common and is achieved by producing micro surface features using photolithography through processes that involve the development of photoresist and exposure to ultraviolet radiation.

2.5 Laser Processing Based Grooving

Laser surface texturing (LST) has recently become a competitive technique to create controlled structures to improve the roughness of surfaces. LST uses high energy pulses to ablate material by rapid melting and vaporizing. Laser ablation can be defined as the removal of material by direct absorption of laser energy on the material surface. The starting of ablation occurs above the threshold fluence has reached. This threshold depends on the micro-structure, morphology, absorption mechanism, material properties, and laser properties, such as wavelength and pulse duration.

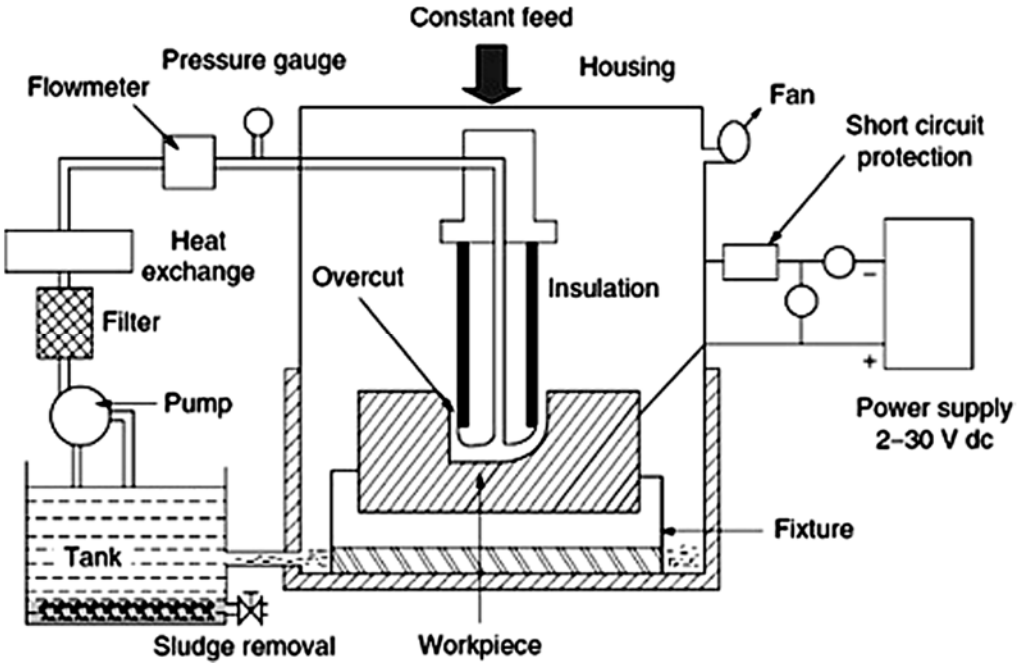

Figure 2.6 Schematic diagram of electrochemical machining (Manikandan et al., 2016).

Laser ablation can be divided into two categories depending upon the interaction of laser energy with the material: pyrolytic and photolytic processes.

In the pyrolytic process, laser energy is absorbed by the material and then transferred into heat, which causes an increase in temperature. As a result, the material melts and evaporates from the surface.

In the photolytic process, the photon energy absorbed induces chemical reactions to overcome the chemical binding energy of molecules; this is also called “cold ablation.”

Some of the important issues regarding LST are; heat-affected zone, surface defects, and the formation of periodical surface structures. Laser beam heat can affect the substrate and cause variations in its metallurgical properties. Frictional behavior of the surface is affected by bulges, as they have significant height. This volume of material is commonly removed from the textured surface by grinding, surface polishing, and lapping. Another issue that has been observed in *ns* and *fs* laser-textured substrate is the formation of periodical surface structures, such as, ripples that cause an increase in the roughness of the surface.

This is recognized as surface acoustic waves or an interference phenomenon. Researchers have used this issue of LST to their advantage to create periodical structures for controlling hydrophobicity of metals, friction, and wear properties of cutting tools.

The way in which the laser beam is projected to the substrate determines the texture accuracy. The methods used are as follows.

(i) A fast-revolving perforated disk is used to practically chop an unfocused laser beam in order to create patterns. However, this technique is generally avoided due to its limited resolution, flexibility, and accuracy.

(ii) A patterned mask is used to split the laser beam projected onto the sample. This technique is flexible, fast, accurate, and allows the creation of various shaped micro-features. The production cost of the mask is the main drawback of this technique.

(iii) A laser beam can be projected using a galvanometric scanner and a computer numerical control (CNC) system, which maneuvers the beam over the sample. This technique is extremely accurate due to the very short pulses (duration of pulse *fs* and *ns*). The main drawback is that this is a time-consuming process, as each texture must be machined separately.

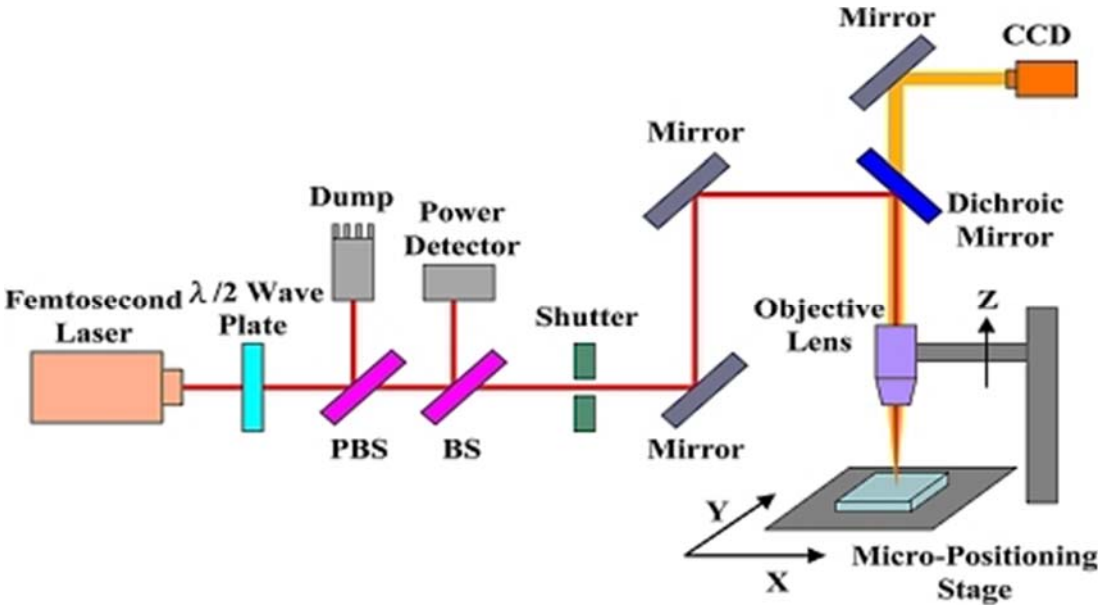

Figure 2.7 Schematic diagram of a femtosecond laser micromachining system.

2.6 Ultrasonic Machining Based Grooving

Ultrasonic machining (USM) is a technique that involves free abrasive particles and a tool. The tool vibrates at ultrasonic frequencies and drives the abrasive particles to produce brittle breakage on the workpiece surface. The basic structure of micro-USM is shown in Fig. 2.8.

The shape and dimensions of the workpiece are determined by the shape and dimensions of the tool. As in USM, material removal is based on brittle breakage, which makes it particularly suitable for machining brittle materials, such as ceramic, glass, graphite, and silicon. Various texture shapes with different dimensions can be obtained with a high degree of accuracy.

Although the microscopic removal phenomenon of micro-EDM is very different from USM, micro-tools are provided in the same way in micro-EDM because the shape of the product is determined by the same type of the tools. The main issues related to CNC USM are material selection, high cost, and a complex 5 axis-CNC control system is required for texturing complex 3D surfaces.

Tribological investigation of textured bearing steel created using USM has been conducted by Shin et al. (2015). They created textures with a diameter of 0.53 mm, a density of 1.37%–2.23%, and a depth of 2 mm–4 mm. They observed a friction coefficient reduction using a density of 1.77% and a depth of 2 mm.

2.7 Focused Ion Beam (FIB) Machining Based Grooving

Focused ion beam machining has attracted a great deal of attention in the production of micro-structured surfaces. FIB milling is the process of producing patterns by direct impingement of the ion beam on the substrate material. FIB can be used for local extraction or deposition with a resolution of nearly 100 nm. Advantages of the FIB method is that it can create micro-structures without using complicated and costly masking and pattern-transfer procedures. The focused ions penetrate the workpiece material and lose their energy while removing workpiece atoms.

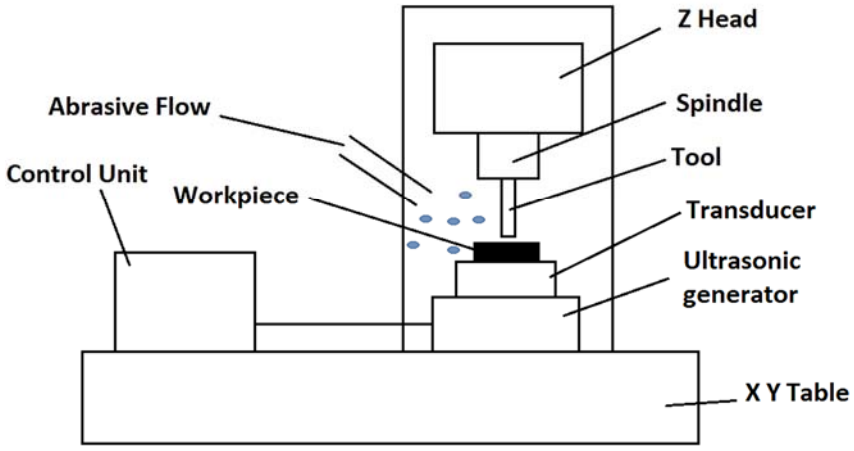

Figure 2.8 Schematic diagram of USM- Ultrasonic machining.

Chang et al. (2011) created micro-grooves on a milling tool using FIB with liquid gallium ion sources. Slot milling trials showed that micro-groove structures improve tool wear resistance. Nakano et al. (2007) also used FIB milling for friction reduction. Using this technique, they created micro- dimples with a diameter of 30 mm and a depth of 11 mm.

The advantages obtained from FIB are high resolution, no restraints on the choice of substrate material, less surface roughness, particularly when FIB is employed for smoothing, and an ion beam spot diameter that provides lateral dimensions to texture . The use of FIB is limited to small-dimension workpieces, as this technique has slow processing speed. Fig. 2.9 shows set up of femtosecond laser micro-machining system.

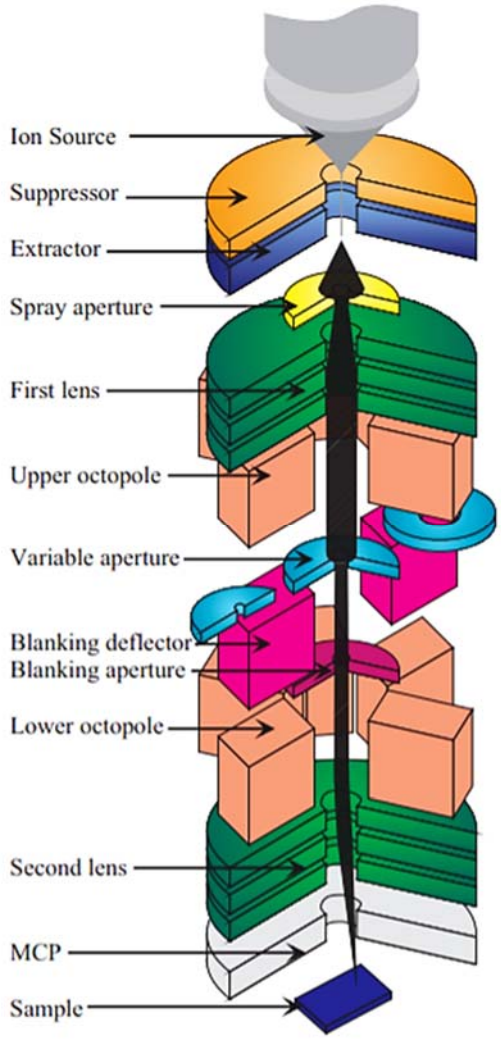

Figure 2.9 Set up of femtosecond laser micro-machining system (Lei et al., 2009).

CHAPTER 3

TURNING WITH MICRO-GROOVED CUTTING TOOLS

This chapter is focused on investigating diagonal micro-grooved tungsten carbide (WC/Co) cutting tool inserts in turning of titanium alloy Ti-6Al-4V. The effect of micro-groove parameters and feed rate on cutting forces and tool wear were studied. For this purpose, the longitudinal (cylindrical) turning of annealed titanium alloy Ti-6Al-4V bars (145.5 mm in diameter) was performed by using TPG432 type insert (insert nose radius of r_ε = 0.8 mm and relief angle of α = 11°) in a rigid CNC turning center. All the tests have been conducted at dry conditions i.e. no coolant or lubricant was used. The inserts were used with a tool holder (Kennametal CTFPR-164C) that provided 0° lead, 0° side rake, and -5° back rake angles. The cutting forces, cutting force F_c, thrust force F_t, and feed force F_f, were measured using Kistler Type 9121 force dynamometer and Kistler Type 9121 turret adapter mounted on the CNC turret disk. The charge signal generated at the dynamometer was amplified using charge amplifiers (Kistler Type 5814B1). The amplified signal is acquired and sampled by using a data acquisition card on a laptop computer at a sampling frequency of 1000 Hz per channel. The experimental configuration along with the micro-grooved tool insert design as well as an in-situ image of chip flow during the turning process is shown in Fig. 3.1.

Diagonal micro-grooves on the tool rake face of tungsten carbide inserts were fabricated with micro EDM milling process using SARIX-μEDM SX100 machine. The groove width (w = 50 μm or 100 μm), spacing between grooves (s = 50 μm, 15 μm or 100 μm), and groove depth (d = 10 μm, 20 μm or 30 μm) were varied for three different inserts. All micro-grooved inserts have a distance between the groove beginning to the cutting edge as t = 100 μm and an orthogonal length of the grooved region as l = 800 μm. The tool design parameters are illustrated in Fig. 3.2.

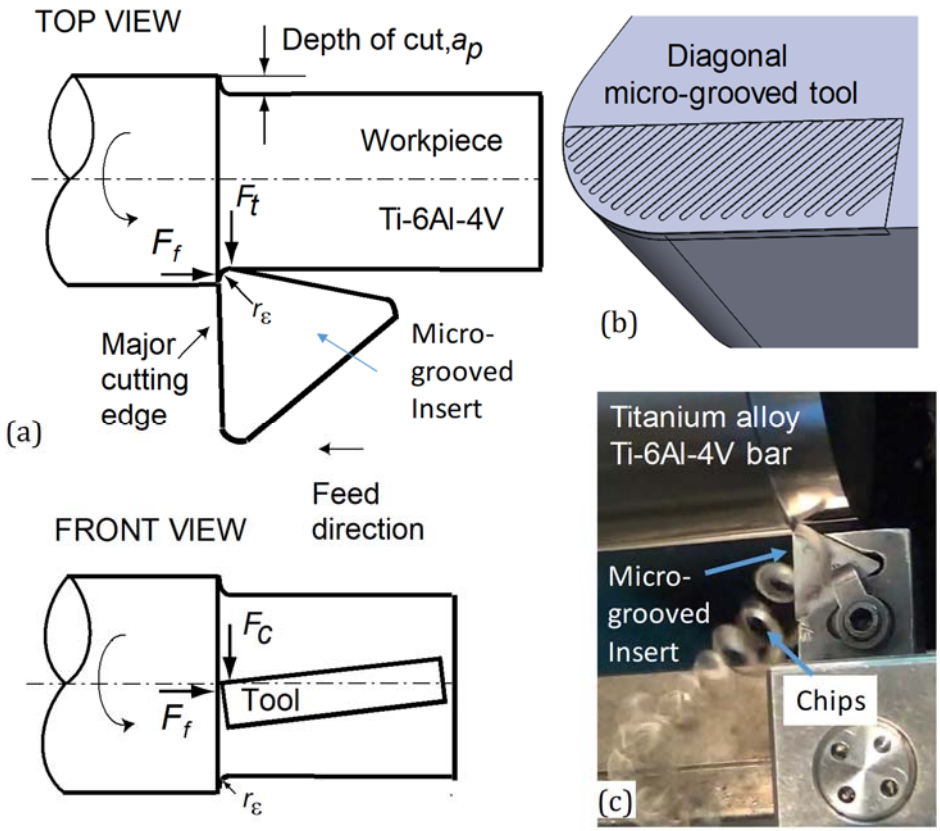

Figure 3.1 Longitudinal turning experimental configuration (a), micro-grooved tool inserts design (b), and in-situ chip flow during experiment (c).

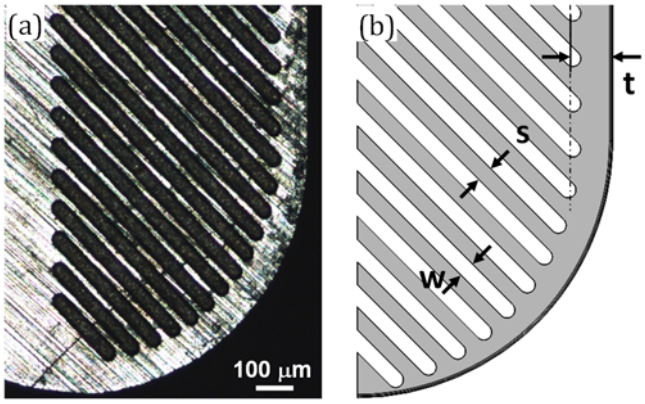

Figure 3.2 Optical microscopy image of the diagonal micro-grooved tool as fabricated (a) and tool design parameter definitions (b), micro-groove parameters; w = 50 μm, s = 15 μm, t = 100 μm, d = 30 μm.

The focused images of the micro-groove spacing section and micro-groove bottom section are shown in Fig. 3.3. It should be noted that the micro-EDM milling

electrode provided a linear (sharp corner) along the side walls of the micro-grooves. But a curvilinear (rounded) surfaces at the bottom of micro-grooves.

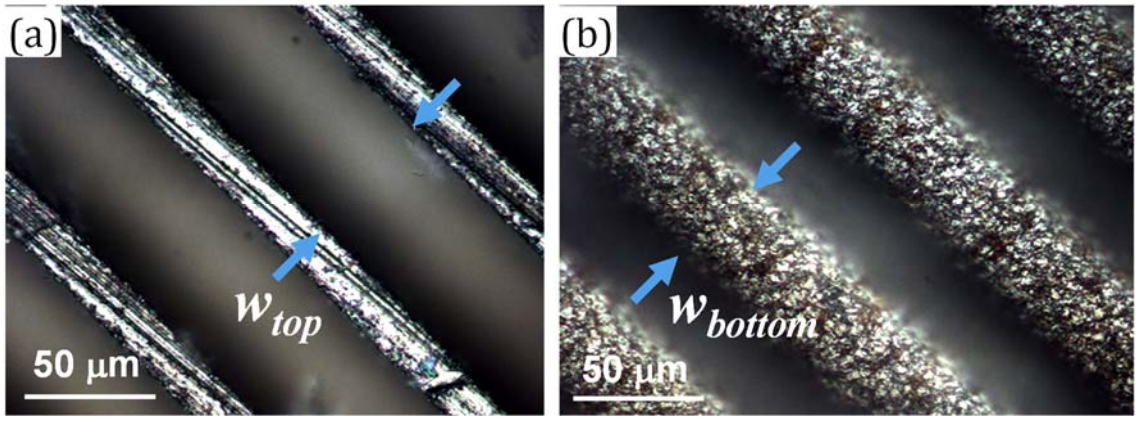

Figure 3.3 Images of micro-grooves at the top (a) and the bottom (b) surfaces (micro-groove parameters; w = 50 µm, s = 15 µm, t = 100 µm, d = 30 µm).

A constant cutting speed (v_c = 90 m/min) and depth of cut (a_p = 2 mm) was selected as cutting condition, while the feed per revolution varied between f = 0.1 mm/rev and f = 0.3 mm/rev. The axial distance of cut kept constant as 0.3929 inches in the feed direction under all cutting conditions. The cutting conditions, including tool designs and cutting parameters, of the longitudinal (cylindrical) turning are, shown in Table 3.1.

Table 3.1 Tool micro-textures designs and cutting parameters for turning experiments.

Test Number	Micro-grooved tool design parameters				Cutting parameters		
	w (µm)	s (µm)	t (mm)	d (µm)	v_c (m/min)	f (mm/rev)	a_p (mm)
1	50	50	0.1	10	90	0.1	2
2	50	50	0.1	10	90	0.2	2
3	50	50	0.1	10	90	0.3	2
4	50	15	0.1	30	90	0.1	2
5	50	15	0.1	30	90	0.15	2
6	50	15	0.1	30	90	0.2	2
7	100	100	0.1	20	90	0.1	2
8	100	100	0.1	20	90	0.15	2
9	100	100	0.1	20	90	0.2	2

3.1 Effect of Feed Rate on Measured Cutting Forces

The results of the turning experiments were utilized to investigate the effect of varying feed rate on the measured cutting forces. The measured cutting forces against the feed rate under different micro-grooved tool designs are shown in Fig. 3.4 through Fig. 3.6. It can be seen that under all different tool designs, the effects of feed rate on the cutting forces were the same, i.e. the cutting forces increased steadily with the increasing feed rate.

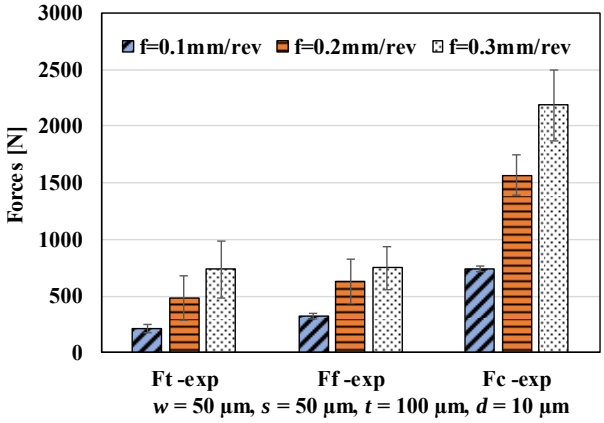

Figure 3.4 Measured cutting forces using micro-grooved tool for varying feed rate, w = 50 µm, s = 50 µm, t = 100 µm, d = 10 µm (v_c = 90 m/min, a_p = 2 mm).

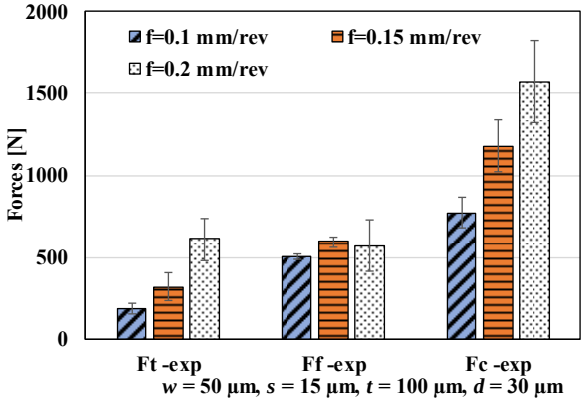

Figure 3.5 Measured cutting forces using micro-grooved tool for varying feed rate, w = 50 µm, s = 15 µm, t = 100 µm, d = 30 µm (v_c = 90 m/min, a_p = 2 mm).

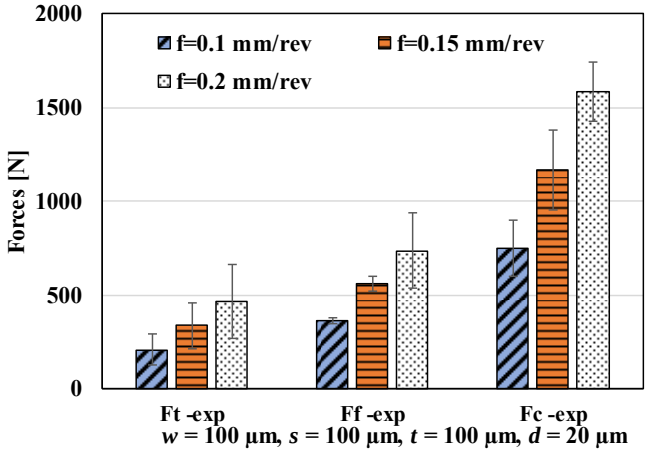

Figure 3.6 Measured cutting forces using micro-grooved tool for varying feed rate, w = 100 µm, s = 100 µm, t = 100 µm, d = 20 µm (v_c = 90 m/min, a_p = 2 mm).

3.2 Effect of Micro-Textured Tools on Tool Wear Behavior

The optical microscopy images of micro-grooved tool rake face after the cutting process are shown in Fig. 3.7 through Fig 3.9. It can be seen that severe wear occurred on the tool rake face during all cutting conditions, and catastrophic tool fracture occurred at some conditions. Smearing material into micro-grooves was found on all insert rake faces. It can also be seen that the degree of wear on the rake face is higher near to the main cutting edge and lowers towards the micro-grooved section, which meant that the tool wear rate varies along the tool-chip contact into the micro-grooved section. The worn areas on the tool rake face were measured along main and trailing cutting edges and are shown. The tool wear was measured when same axial distance of cut was taken under all cutting conditions. The wear along rake face can represent the effect of feed rate.

Furthermore, areal surface height maps were obtained from rake faces of micro-grooved tool inserts by using focus variation microscopy (FVM) system (Alicona InFocus G4 XL200) as shown in Fig. 3.10 through 3.12. These areal height maps provide further details about crater wear depth, edge wear depth, locations of chip smearing into micro-grooves and material adhesion, and chipping. The cutting conditions at high feed rate resulted in some chipping of the cutting edge but also

chip smearing and material adhesion have been observed almost all cutting conditions and micro-grooved tool designs.

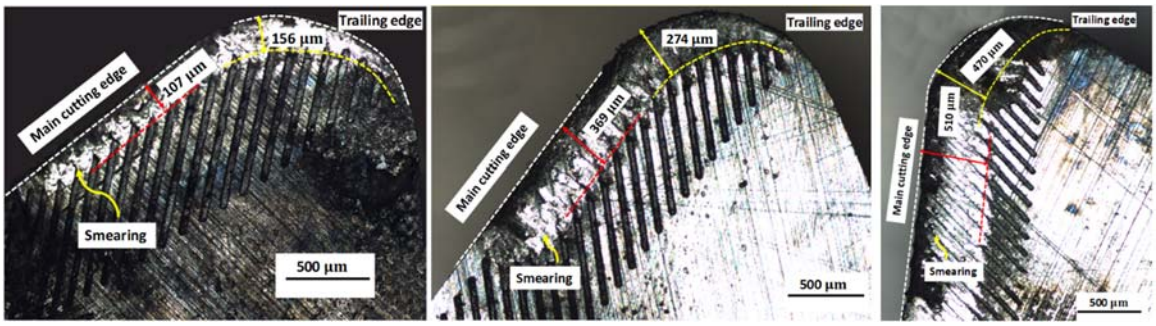

Figure 3.7 (a) Test No. 1 (f = 0.1 mm/rev) (b) Test No. 2 (f = 0.2 mm/rev) (c) Test No. 3 (f = 0.3 mm/rev) [w = 50 µm, s = 50 µm, t = 100 µm, d = 10 µm]

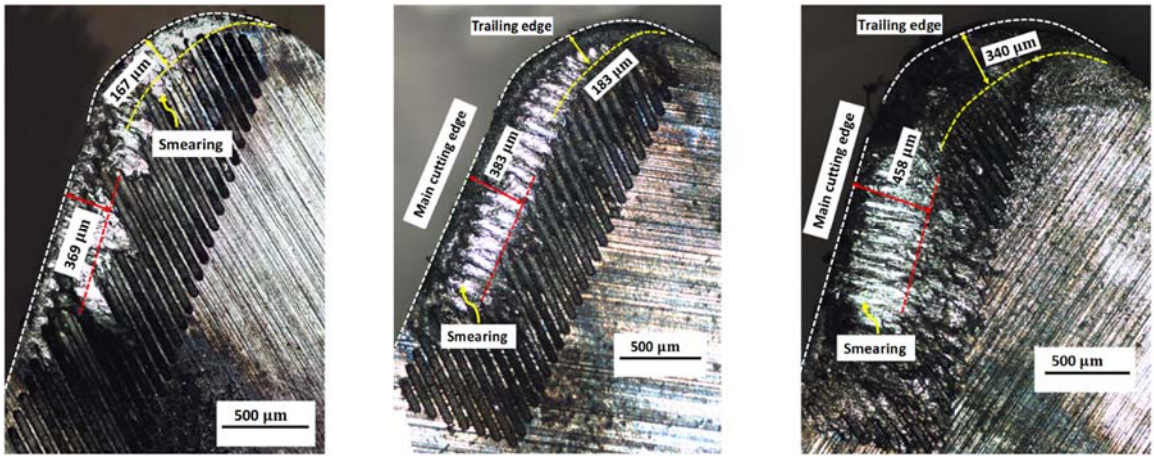

Figure 3.8 (d) Test No. 4 (f = 0.1 mm/rev) (e) Test No. 5 (f = 0.15 mm/rev) (f) Test No. 6 (f = 0.2 mm/rev) [w = 50 µm, s = 15 µm, t = 100 µm, d = 30 µm]

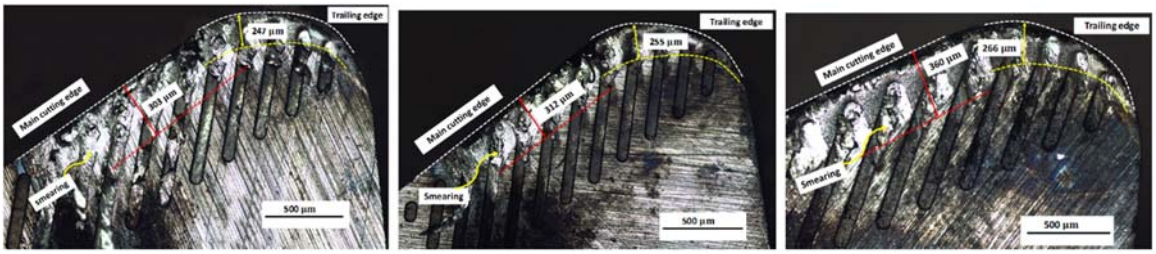

Figure 3.9 (g) Test No. 7 (f = 0.1 mm/rev) (h) Test No. 8 (f = 0.15 mm/rev) (i) Test No. 9 (f = 0.2 mm/rev) [w = 100 µm, s = 100 µm, t = 100 µm, d = 20 µm]

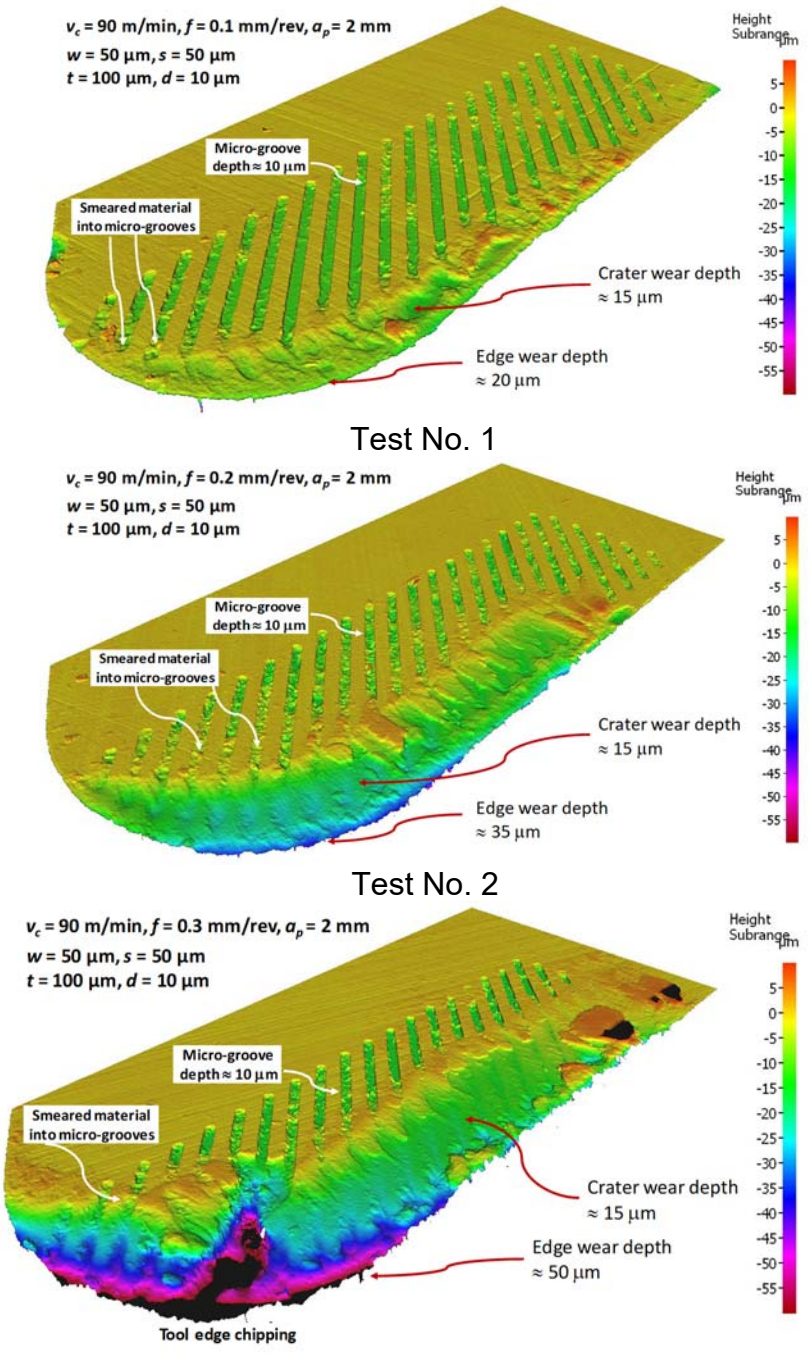

Figure 3.10 The areal height maps obtained from micro-grooved tool rake faces after cutting process. (a) Test No. 1 (f = 0.1 mm/rev), (b) Test No. 2 (f = 0.2 mm/rev), (c) Test No. 3, (f = 0.3 mm/rev). [w = 50 µm, s = 50 µm, t = 100 µm, d = 10 µm]

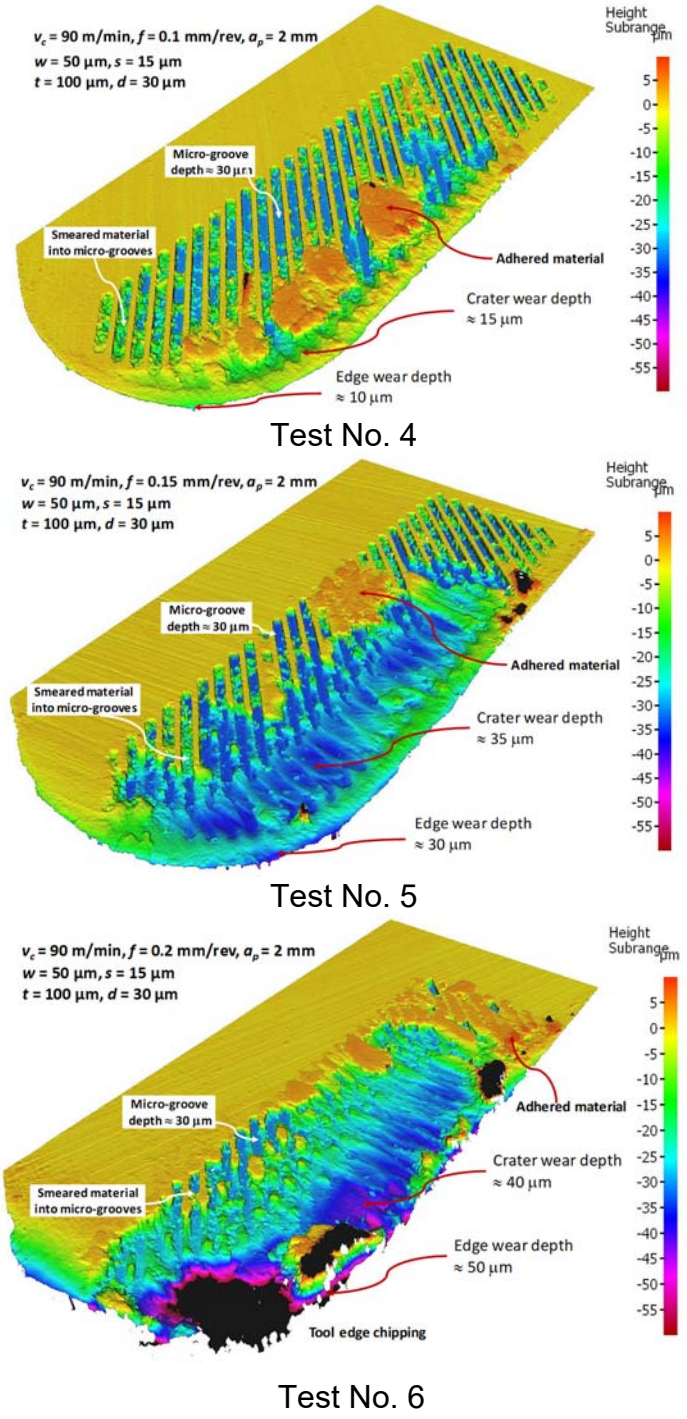

Figure 3.11 The areal height maps obtained from micro-grooved tool rake faces after cutting process. (g) Test No. 7 (f = 0.1 mm/rev), (h) Test No. 8 (f = 0.15 mm/rev), (i) Test No. 9 (f = 0.2 mm/rev) [w = 100 µm, s = 100 µm, t = 100 µm, d = 20 µm]

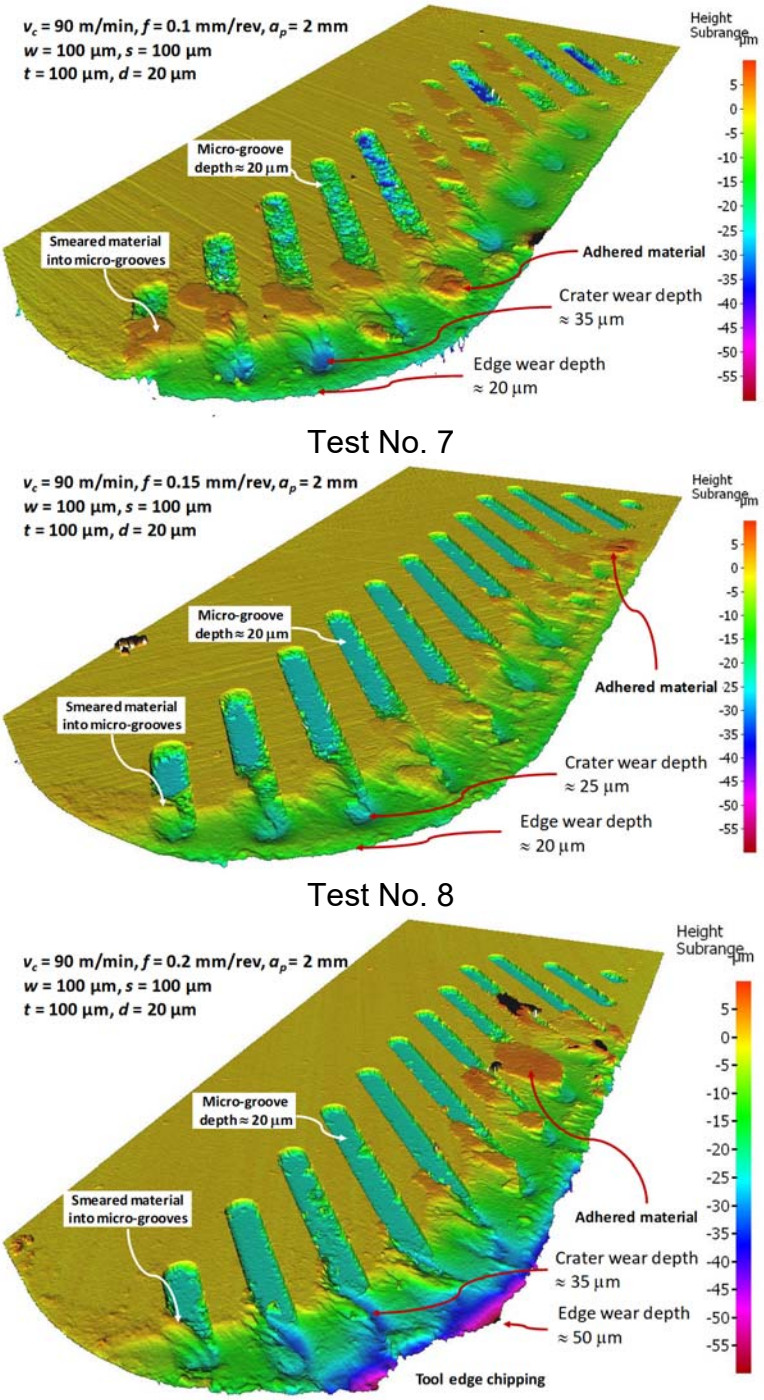

Figure 3.12 The areal height maps obtained from micro-grooved tool rake faces after cutting process. (g) Test No. 7 (f = 0.1 mm/rev), (h) Test No. 8 (f = 0.15 mm/rev), (i) Test No. 9 (f = 0.2 mm/rev) [w = 100 µm, s = 100 µm, t = 100 µm, d = 20 µm]

The effect of feed rate on the tool rake face wear length with different micro-grooved tool designs is investigated in Fig. 3.13. It can be seen that the effect of feed rate on the tool rake face wear length is the same on all micro-grooved tool designs, i.e. the tool rake face wear length increased overall with increasing feed rate. As cylindrical bar turning configuration suggests (Fig. 3.1), the increased feed rate will result in larger undeformed chip thickness on the tool rake face in the direction against the main cutting edge. Therefore, the tool rake face wear length will increase as well. In addition, the increased feed rate generated higher cutting forces, which also resulted in more severe tool rake face wear and even tool fracture around the tool cutting edge region. This can be seen in Fig. 3.13 through Fig. 3.15.

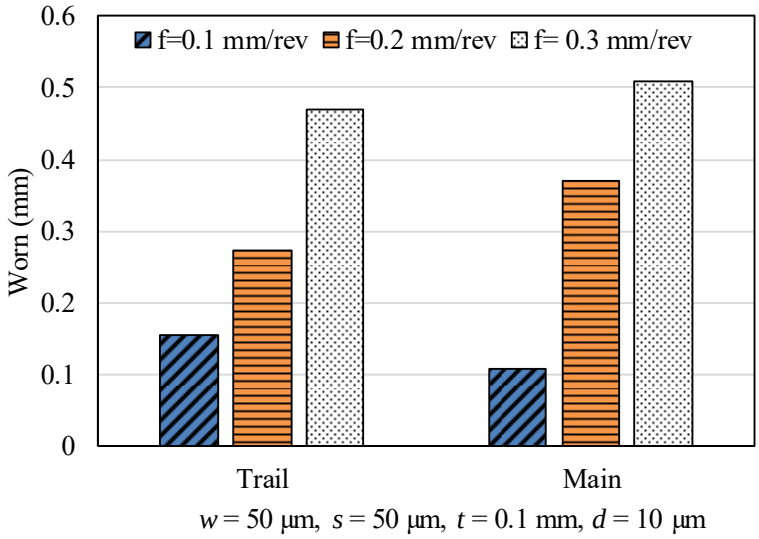

Figure 3.13 Measured tool wear on the micro-grooved tool for varying feed rate, w = 50 µm, s = 50 µm, t = 100 µm, d = 10 µm (v_c = 90 m/min, a_p = 2 mm).

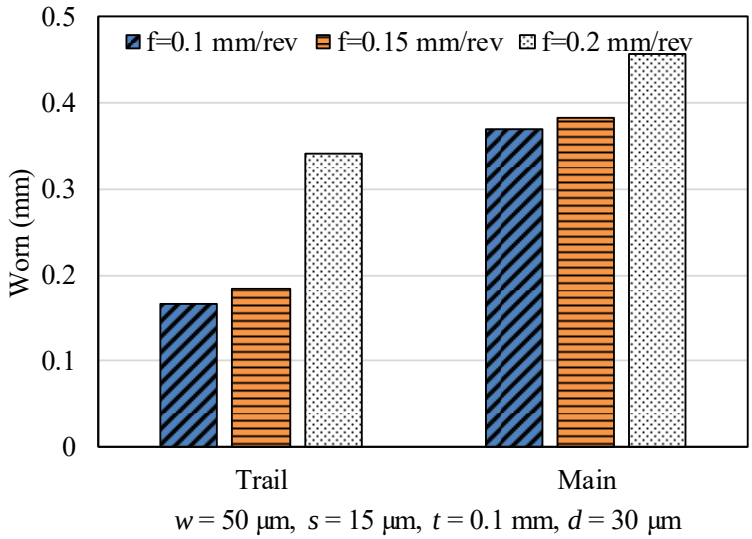

Figure 3.14 Measured tool wear on the micro-grooved tool for varying feed rate, w = 50 µm, s = 15 µm, t = 100 µm, d = 30 µm (v_c = 90 m/min, a_p = 2 mm).

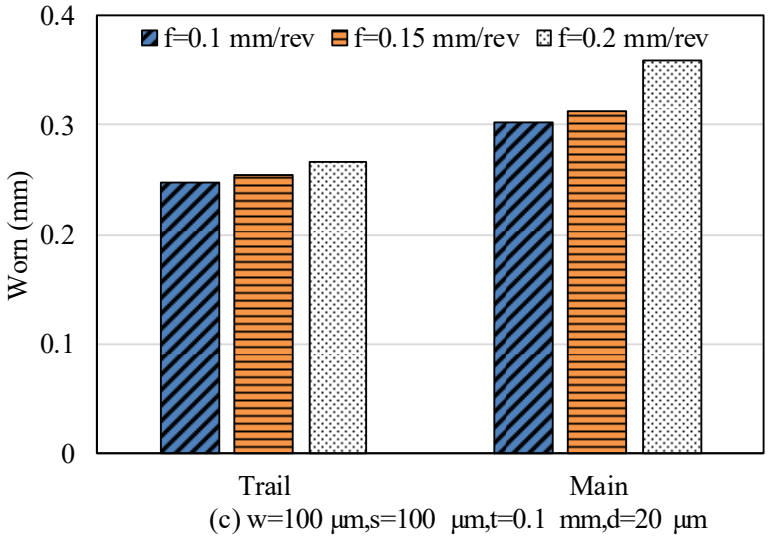

Figure 3.15 Measured tool wear on the micro-grooved tool for varying feed rate, w = 100 µm, s = 100 µm, t = 100 µm, d = 20 µm (v_c = 90 m/min, a_p = 2 mm).

With the help of Alicona Imaging GmbH, we measured the volume above and below the surface of the tool. These results helped us to understand the wear and smearing of material on the face of the tool. The volume above the surface represents the extra material which is sticking to the tool surface and volume below the surface will give us an idea about the wear. One important thing is that volume below the surface is also consisting of the groove itself as well because they are

also engraved and hence below the surface. Though they will give us the idea about the wear at the cutting edge. The images below show the volumetric measurements. The area in red is below the surface and rest is above the surface.

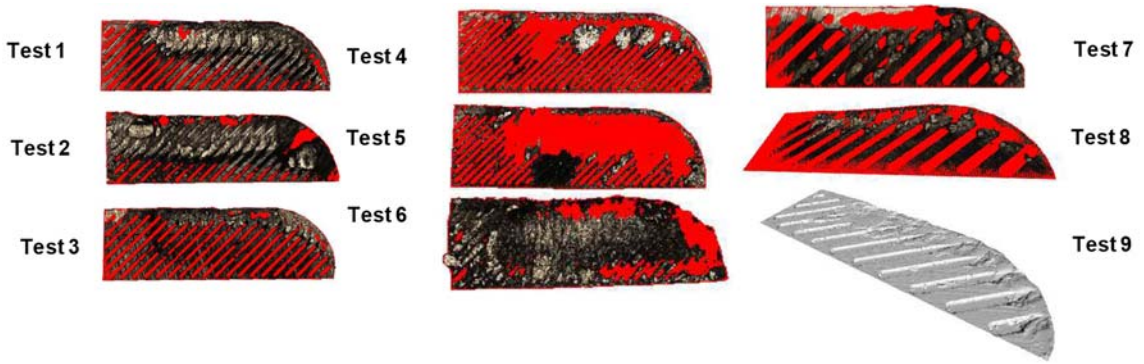

Figure 3.16 Volumetric measurements on the micro-grooved tool for various test conditions.

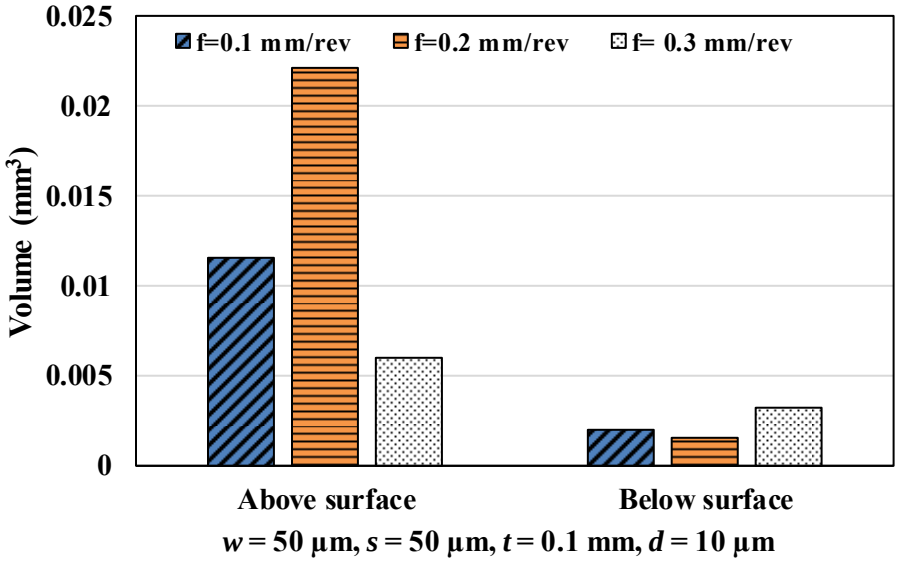

Figure 3.17 Volumetric measurements on the micro-grooved tool for varying feed rate, w = 50 µm, s = 50 µm, t = 100 µm, d = 10 µm (v_c = 90 m/min, a_p = 2 mm).

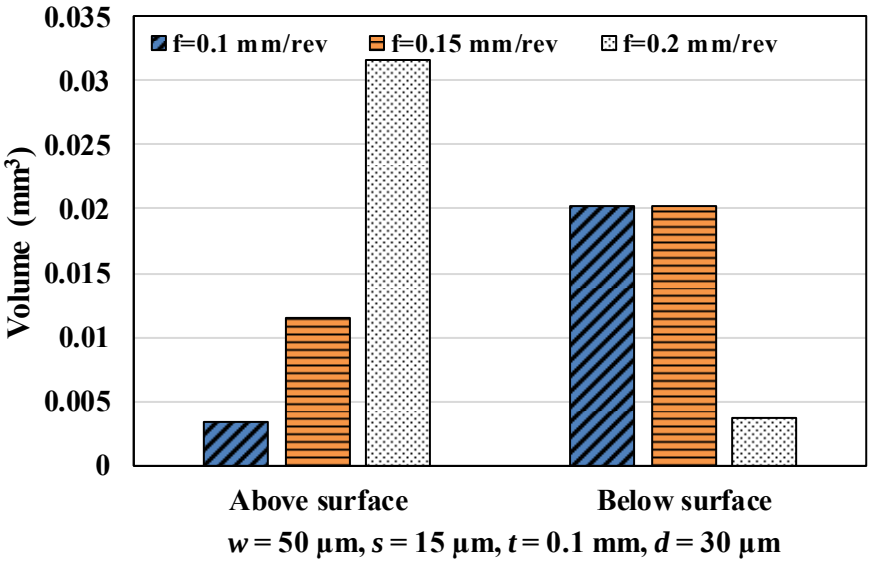

Figure 3.18 Volumetric measurements on the micro-grooved tool for varying feed rate, w = 50 µm, s = 15 µm, t = 100 µm, d = 30 µm (v_c = 90 m/min, a_p = 2 mm).

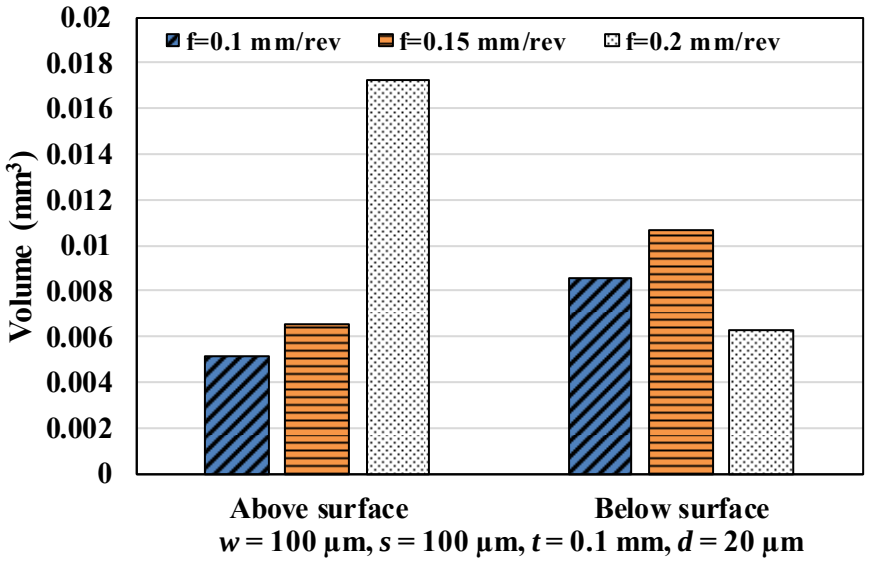

Figure 3.19 Volumetric measurements on the micro-grooved tool for varying feed rate, w = 100 µm, s = 100 µm, t = 100 µm, d = 20 µm (v_c = 90 m/min, a_p = 2 mm).

CHAPTER 4

ORTHOGONAL CUTTING WITH MICRO-GROOVED CUTTING TOOLS

This work is focusing on testing micro-grooved tungsten carbide (WC/Co) cutting tool inserts in the orthogonal cutting of alloy steel 4340. The effect of micro-groove parameters, cutting speed, and feed rate on cutting forces and tool wear were studied. For this purpose, the orthogonal turning of thin webs on the annealed alloy steel 4340 was performed by using TPG432 type insert (insert cutting edge radius of r_β = 5 μm and relief angle of α = 11°) in a rigid CNC turning center (Fig. 4.1).

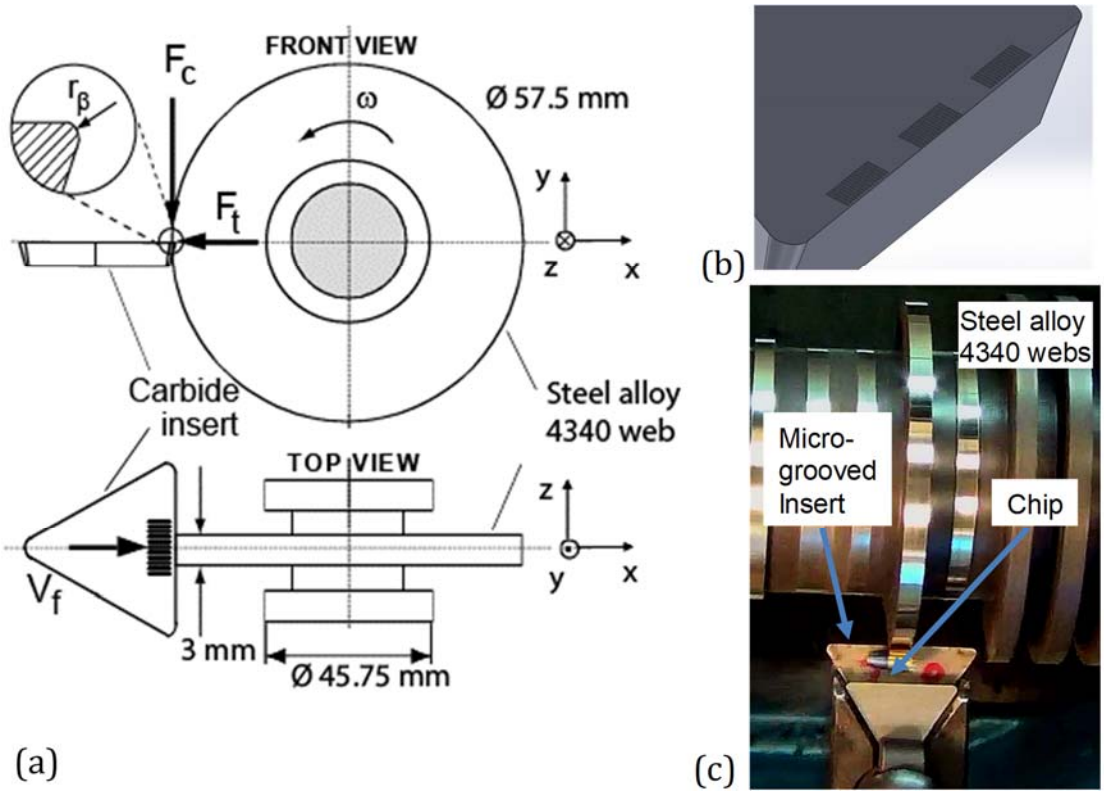

Figure 4.1 Orthogonal turning experimental configuration (a), micro-grooved tool inserts design (b), and in-situ chip flow during experiment (c).

All the tests have been conducted at dry conditions i.e. no coolant or lubricant was used. The inserts were used with a tool holder (Kennametal CTCDN 64-4F) that provided 0° rake angles. The cutting forces were measured with a force dynamometer (Kistler Type 9121) mounted on the turret disk of the CNC turning center and acquired with a charge amplifier (Kistler Type 5814B1) and a data acquisition card on a laptop computer at a sampling frequency of 1000 Hz per

channel. The experimental configuration along with the micro-grooved tool insert as well as resultant in-situ chip flow is shown in Fig. 4.1. In this figure, the cutting force is F_c and the thrust force is F_t.

In this study, diagonal micro-grooves on the tool rake face of tungsten carbide inserts were fabricated with μ-EDM milling process using SARIX-μEDM SX100 machine. The groove width (w = 50 μm, 100 μm), spacing between the grooves (s = 50 μm, 75 μm, 100 μm, 150 μm, 200 μm), and the groove depth (d = 10 μm, 20 μm, 30 μm) were varied for three different triangular inserts with a total of 27 cutting edges. All micro-grooved inserts have a distance from the groove beginning to the cutting edge as t = 100 μm and an orthogonal length of the grooved region as l = 500 μm. The tool design parameters are illustrated on micro-grooved tool design in Fig. 4.2.

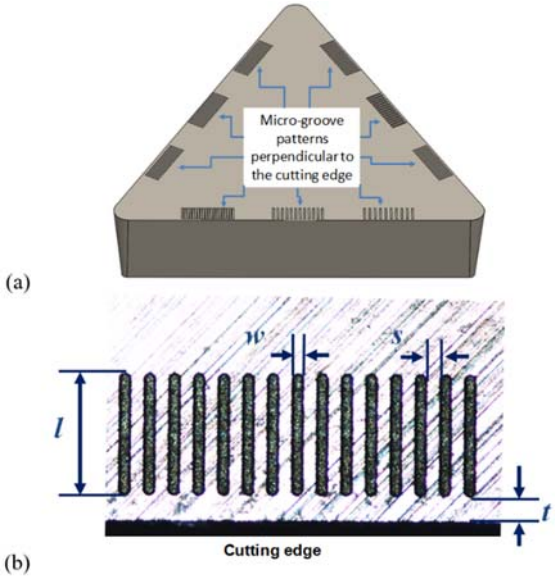

Figure 4.2 Layout of the micro-groove patterns on the cutting tool insert geometry (a), an optical microscopy image of a section of the micro-grooved tool as fabricated with micro-groove parameter definitions (l = 500 μm, w = 50 μm, s = 50 μm, t = 100 μm) (b).

In the tests, the cutting speed was varied (v_c = 25 m/min, 75 m/min, 125 m/min) and the feed per revolution varied (f = 0.1 mm/rev, 0.125 mm/rev, 0.15 mm/rev). A total of 27 different micro-grooved parameters were tested to investigate the effect of micro-groove spacing, micro-groove depth, and micro-groove width on cutting

forces and tool wear. The micro-groove parameters and cutting parameters are shown in Table 4.1.

Table 4.1 Micro-groove and cutting parameters.

Test No.		**Micro-groove parameters**			**Cutting parameters**		**Specific Cutting forces**		**Friction coefficient**
	w [μm]	s [μm]	t [μm]	d [μm]	v_c [m/min]	f [mm/rev]	K_c [N/mm^2]	K_t [N/mm^2]	μ [-]
1	50	50	94	10	125	0.1	4095.2	2186.1	0.53
2	50	75	97	10	125	0.15	4697.1	2473.2	0.53
3	50	100	99	10	125	0.2	4578.8	2747.3	0.60
4	50	50	94	10	125	0.1	4315.0	2293.1	0.53
5	50	75	96	10	125	0.125	5235.8	2811.4	0.54
6	50	100	98	10	125	0.15	5641.9	3735.5	0.66
7	50	50	93	30	25	0.1	2616.8	1190.3	0.45
8	50	50	94	30	25	0.125	2683.7	1246.8	0.46
9	50	50	95	30	25	0.15	2691.8	1475.3	0.55
10	50	50	97	30	75	0.1	6137.0	3092.3	0.50
11	50	50	98	30	75	0.125	5775.0	3629.0	0.63
12	50	50	100	30	75	0.15	6351.8	3920.2	0.62
13	100	100	100	20	25	0.1	2693.3	1642.1	0.61
14	100	150	95	20	25	0.125	2704.6	1387.3	0.51
15	100	200	96	20	25	0.15	2565.7	1351.3	0.53
16	100	200	99	20	75	0.1	3553.3	2685.8	0.76
17	100	100	97	20	75	0.125	6221.8	4373.5	0.70
18	100	150	100	20	75	0.15	6182.9	3458.7	0.56
19	50	50	96	10	75	0.1	5617.0	2644.7	0.47
20	50	75	100	10	75	0.125	4848.5	2639.6	0.54
21	50	100	95	10	75	0.15	4785.1	2297.8	0.48
22	50	50	93	30	25	0.1	2558.8	1498.2	0.59
23	50	50	94	30	25	0.125	2586.7	1439.9	0.56
24	50	50	96	30	25	0.15	2551.9	1266.4	0.50
25	100	100	95	20	125	0.1	3405.3	1912.4	0.56
26	100	150	95	20	125	0.125	4913.1	2213.4	0.45
27	100	200	100	20	125	0.15	6093.0	2804.1	0.46

4.1 Force Measurement Results and Discussions

4.1.1 Effects of Micro-Texture on Measured Cutting Forces

The results of the orthogonal cutting experiments were utilized to investigate the effect of varying cutting speed and feed rate on the measured cutting forces with respect to the different micro-groove parameters. The effects of micro-groove width (w) on measured specific forces against the increasing feed rate under different micro-groove spacing values (s) are shown in Fig. 4.3 at two cutting speed levels (v_c = 125 m/min and v_c = 75 m/min). The effects of micro-groove depth (d) on measured specific forces against the increasing feed rate under different micro-groove spacing values (s) are shown in Fig. 4.4 at two cutting speed levels (v_c = 75 m/min and v_c = 25 m/min). Effects of micro-groove parameters on measured specific forces were seen to be the same at lower feed rate (f = 0.1 mm/rev). This is because; most of the chip load was received at the non-textured section on the rake face because the texture pattern distance from the cutting edge (t = 0.1 mm) is same as feed per revolution. However, measured cutting forces increased steadily with the increasing feed rate and it seems that forces are less affected by micro-groove depth.

Since a varying width and spacing is used for all micro-grooved tool insert sections, the effect of the micro-groove width and spacing was found to be significant on measured cutting forces. At the highest cutting speed (v_c = 125 m/min) tested (Fig. 4.3 a-b), specific cutting forces (both K_c and K_t) were lowered with increasing micro-groove width and spacing. However, at the lower cutting speed (v_c = 125 m/min) this trend was reversed (Fig. 4.3 c-d).

The effect of micro-groove depth on the specific cutting forces indicates that increasing groove depth increased specific forces when same micro-groove width and spacing parameters were applied. This is perhaps due to chip smearing deeper into micro-grooves and increasing forces during cutting. At the cutting speed of v_c = 75 m/min, cutting with tools micro-grooved with a depth of d = 30 μm resulted at higher specific forces (Fig. 4.4 a-b). This effect was found to be less

observable or even reversed when cutting speed is lowered down to v_c = 25 m/min (Fig. 4.4 c-d).

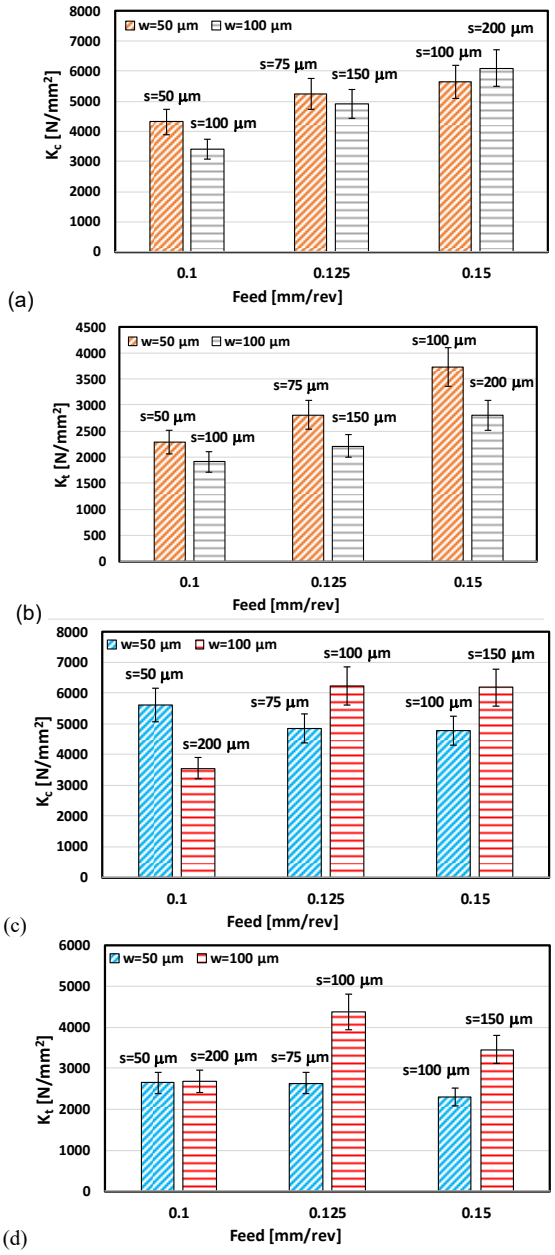

Figure 4.3 Effects of micro-groove width and spacing on measured specific cutting forces of K_c (a) and K_t (b) at v_c = 125 m/min and K_c (c) and K_t (d) at v_c = 75 m/min with varying feed rate per unit width of cut and feed.

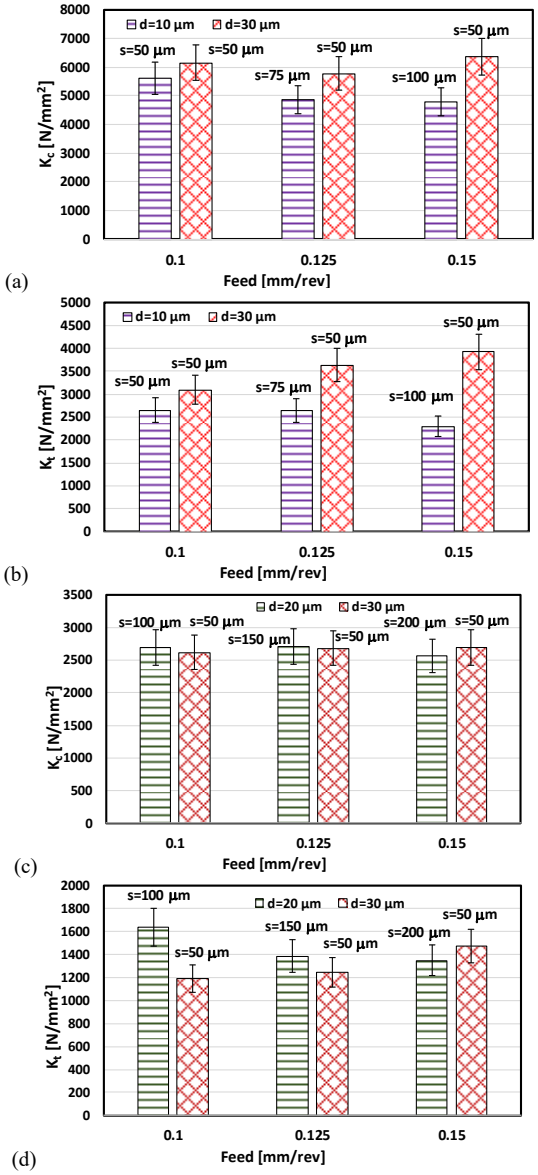

Figure 4.4 Effects of micro-groove depth and spacing on measured specific forces of K_c (a) and K_t (b) at v_c = 75 m/min and K_c (c) and K_t (d) at v_c = 25 m/min with varying feed rate per unit width of cut and feed.

All friction coefficients were found to be between 0.45 and 0.76 with an average of 0.55 and a standard deviation of 0.07. Average friction coefficients of 0.53, 0.54, and 0.58 were found for cutting speeds of 25 m/min, 75 m/min, and 125 m/min respectively. Which are low compared to general Non-textured tool cutting conditions. Which proves our texture has some effect on the frictional forces in cutting action.

In fact, According to Zorev's assumed distribution of normal pressure *p* on the rake surface of cutting tool has the distribution as shown in Fig. 4.5. Fig. 4.5(a) shows Zorev's assumed distribution of normal pressure *p* and shear stress *τ* on the rake face of a tool, for a given (*s*/*L*), in which *n*>1 (Zorev 1963). Where in Fig. 4.5(b) the less-familiar distribution where *n*<1, which applies when the sticking zone occupies a large proportion of the rake face, i.e. when (*s*/*L*) is large. When (*s*/*L*) =1, *n*=0 so that *p* and *τ* are then constant along the whole rake face. In these diagrams, *k* is shown constant and ignores work hardening since along the rake face material is almost perfectly plastic in its behavior If our texture falls within sticking region of machined chip, it will generate less friction due to less contact. Which can be understood by Fig. 2.3.

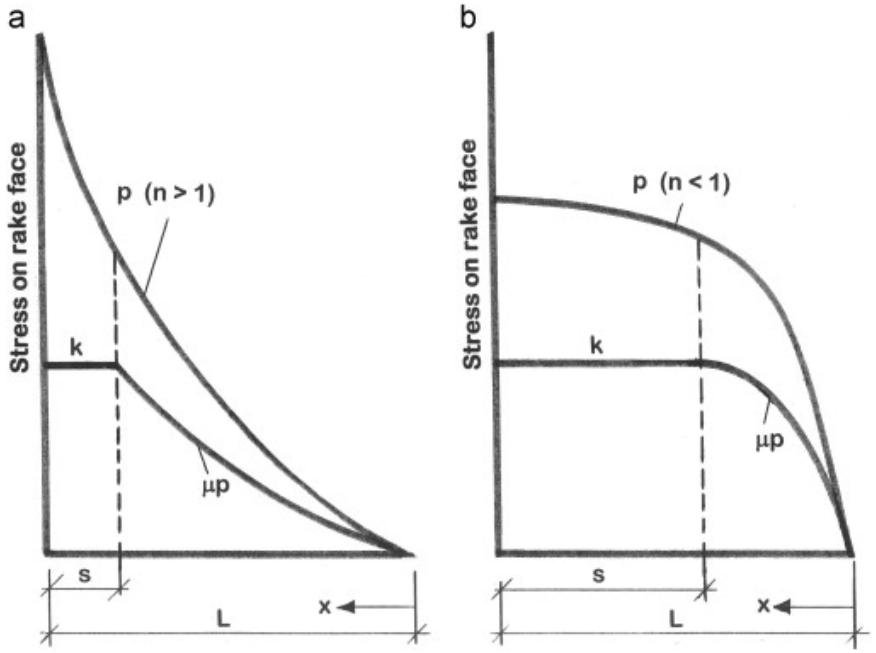

Figure 4.5 Zorev's assumed distribution of normal pressure *p* on rake surface.

Higher stress values and high friction will generate more temperature near cutting edge. The temperature will reduce when the distance increase from the edge. This high temperature and stresses will prevent us from making texture right on the

edge because it will destroy the texture very early causing the high tool wear and very short tool life.

In some case under high feed per evolution, sudden fracture of the cutting edge was observed which was caused by this high temperature and pressure. The wear behavior of the micro-textured tools is explained in the next section.

4.1.2 Effects on Tool Wear and Chip Smearing

The optical microscopy images of micro-grooved tool rake face after the cutting process are shown in Fig. 4.6. Tool wear was measured only on the rake faces of textured cutting tools by measuring the distance on the surface marks left by the chips. These wear regions were measured as; (i) chip smearing length (l_{smearing}) where chips adhered and smeared into micro-grooves, (ii) severe wear length (l_{severe}) where chips left severe marks on the rake face, and (iii) sliding wear length (l_{sliding}) where chips left sliding wear marks.

Addition of sliding and severe wear will give total wear on rake face. Severe wear incurred on the tool rake face during all cutting conditions. Smearing of chips into micro-grooves was found on all insert rake faces. It can also be seen that the degree of wear on the rake face is higher near to the main cutting edge and lowers toward the micro-grooved section, which meant that the tool wear rate varies along the tool-chip contact into the micro-grooved section. The worn areas on the tool rake face were measured along the cutting edge as indicated in Fig. 4.6.

These three distinct tool wear lengths were measured when the same distance of cut was taken under all cutting conditions as given in Fig. 4.7. The wear along rake face can represent the effect of feed rate. The effects of micro-groove spacing, and micro-groove depth were also observable that a larger micro-groove width resulted in higher amount of chip material smearing into the micro-grooves. A higher sliding wear is seen for larger micro-groove spacing.

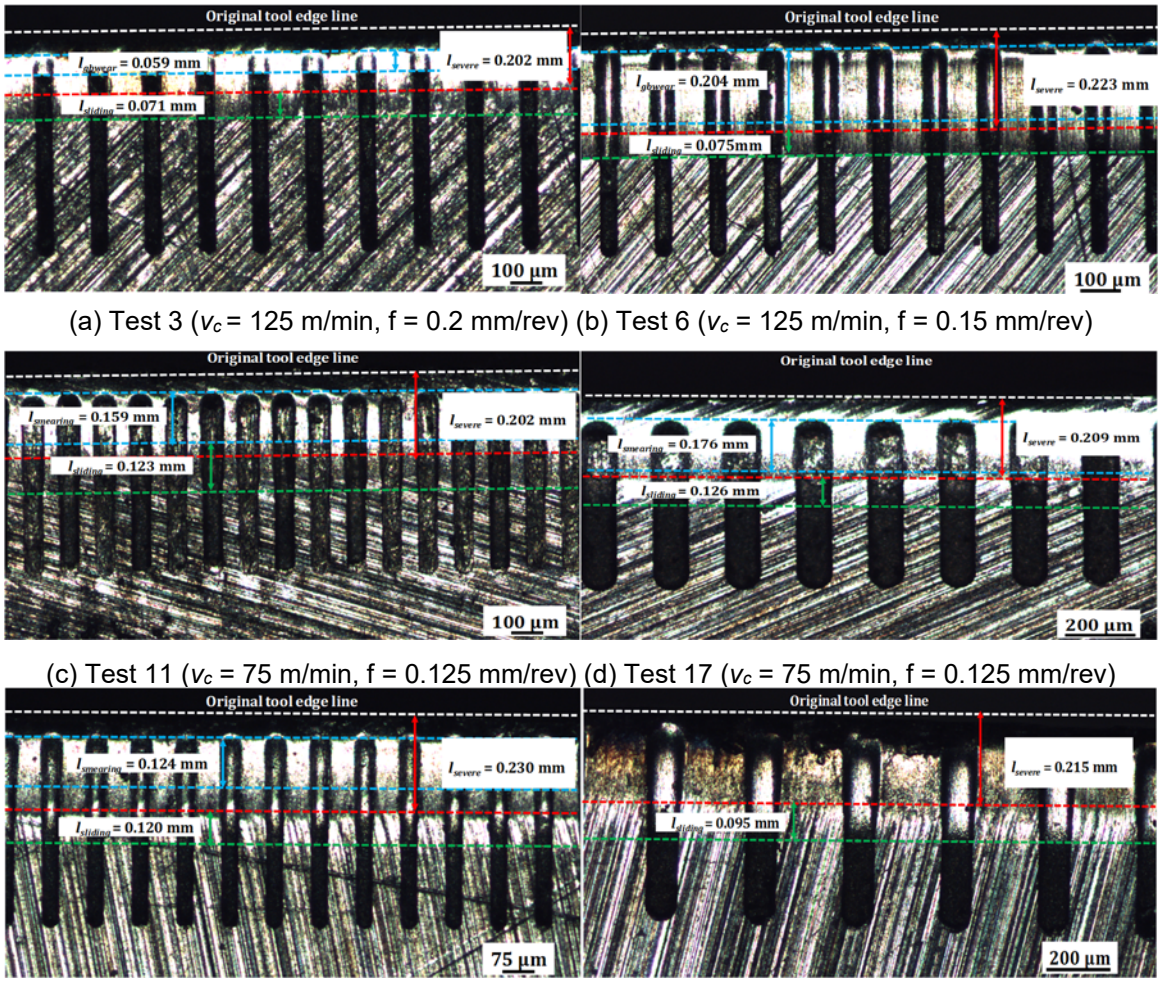

(a) Test 3 (v_c = 125 m/min, f = 0.2 mm/rev) (b) Test 6 (v_c = 125 m/min, f = 0.15 mm/rev)

(c) Test 11 (v_c = 75 m/min, f = 0.125 mm/rev) (d) Test 17 (v_c = 75 m/min, f = 0.125 mm/rev)

(e) Test 20 (v_c = 75 m/min, f = 0.125 mm/rev) (f) Test 27 (v_c = 125 m/min, f = 0.15 mm/rev)

Figure 4.6 Optical microscopy images of tool rake face with measured wear.

These three distinct tool wear lengths were measured when the same distance of cut was taken under all cutting conditions as given in Fig. 4.7. The wear along rake face can represent the effect of feed rate. The effects of micro-groove spacing, and micro-groove depth were also observable that a larger micro-groove width resulted in higher amount of chip material smearing into the micro-grooves. A higher sliding wear is seen for larger micro-groove spacing.

Furthermore, areal surface height maps were obtained from rake faces of micro-grooved tool inserts by using focus variation microscopy (FVM) system (Alicona InFocus G4 XL200) as shown in Figs. 4.8-4.10. Focus variation technique

combines the small depth of focus of an optical system with vertical scanning to provide topographical and color scaling information from the variation of focus.

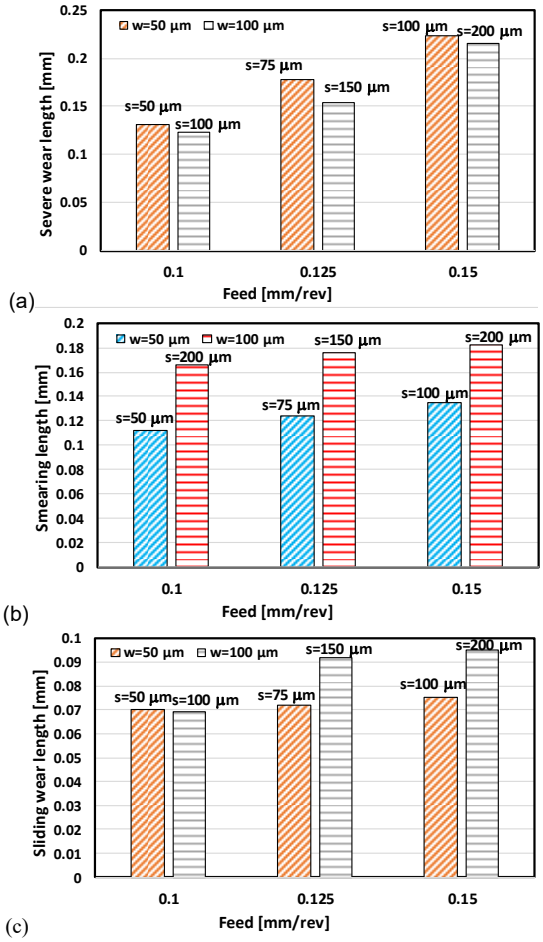

Figure 4.7 Tool rake face wear measured against the feed rate at cutting speed of v_c =125 m/min.

These areal height maps provide further details about crater wear depth, edge wear depth, locations of chip smearing into micro-grooves and material adhesion, and tool edge chipping. The cutting conditions at high cutting speeds resulted in less smearing and at high feed rate resulted in some chipping of the cutting edge but also chip smearing and material adhesion have been observed almost all cutting conditions and micro-grooved tool designs. Steel alloy 4340 material that is smearing in micro-grooves show evidence of chip flow following along micro-groove directions and distribution of chip-tool contact over micro-grooved surfaces.

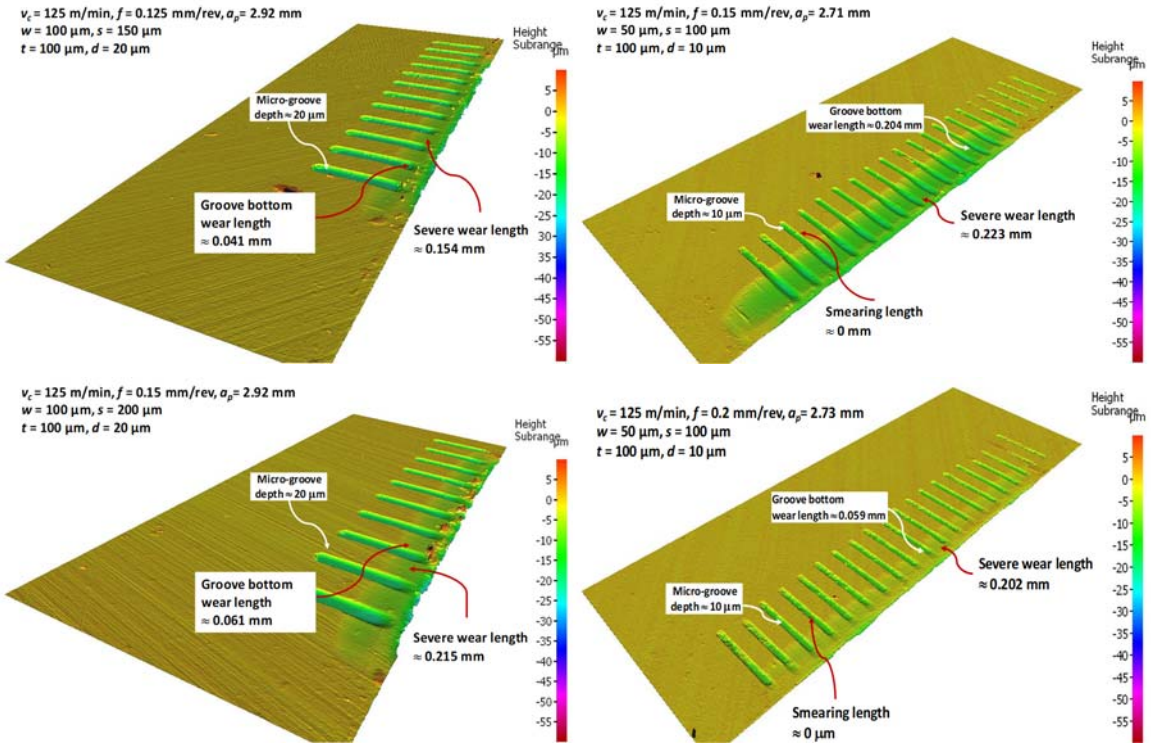

Figure 4.8 The areal height maps obtained from micro-grooved rake faces with measured wear (tests at v_c = 125 m/min).

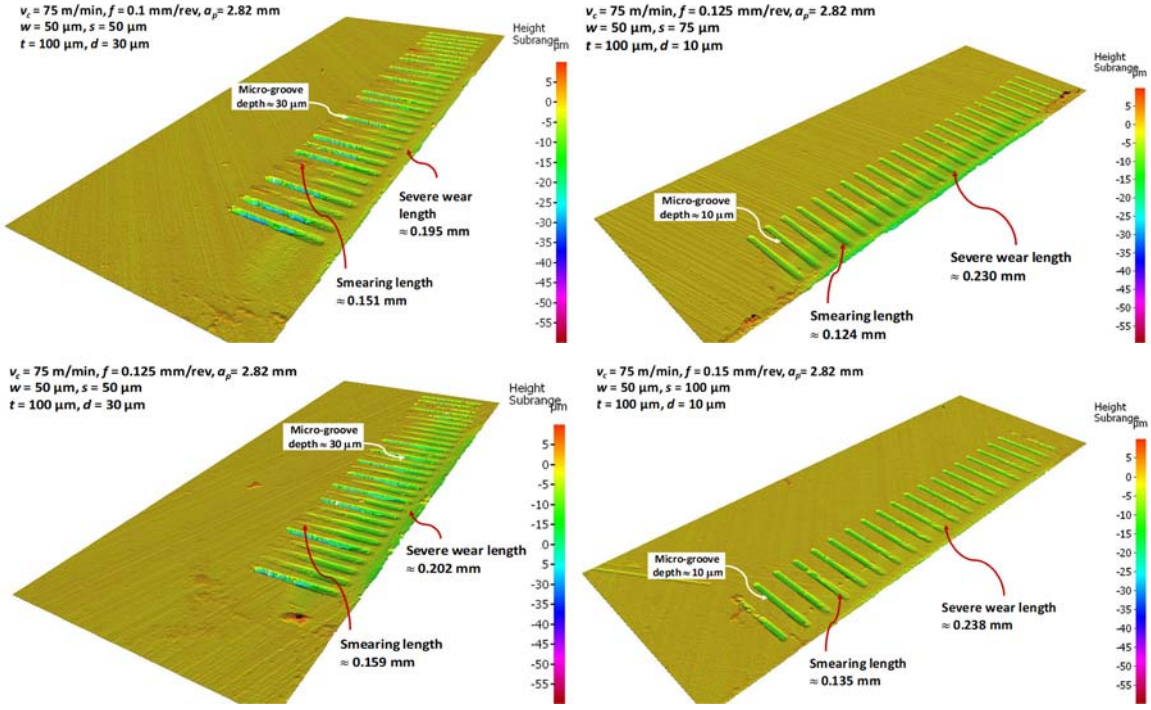

Figure 4.9 The areal height maps obtained from micro-grooved rake faces with measured wear (tests at v_c = 75 m/min).

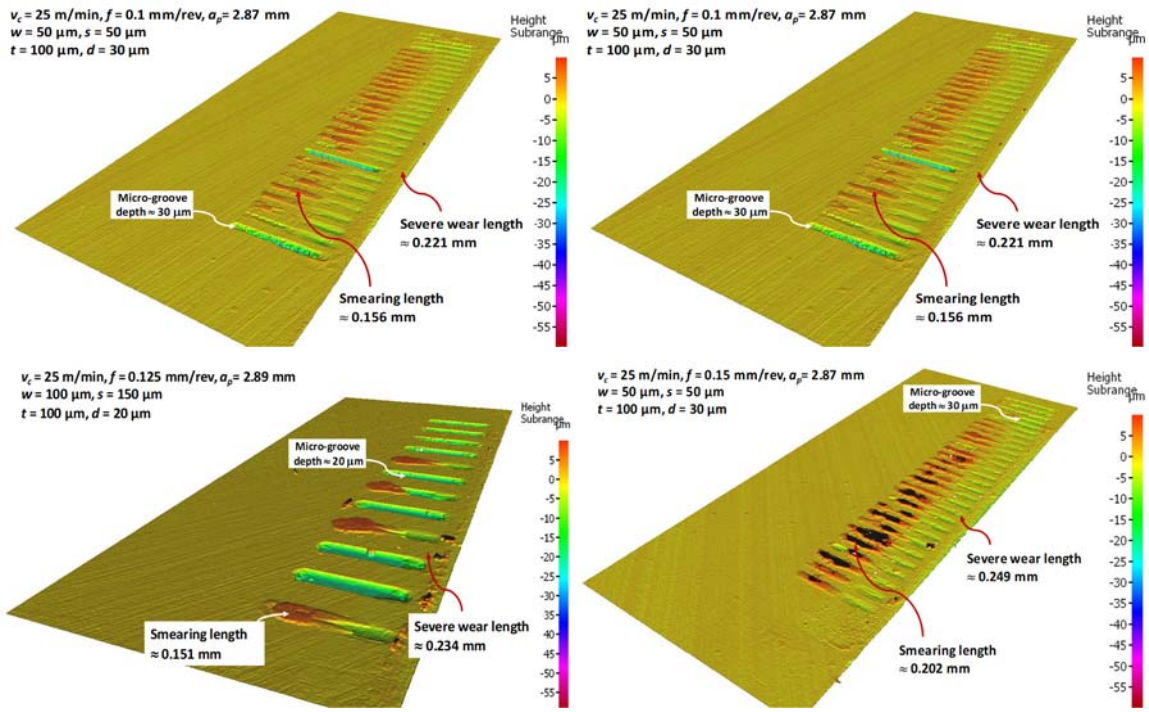

Figure 4.10 The areal height maps obtained from micro-grooved rake faces with measured wear (tests at v_c = 25 m/min).

CHAPTER 5

EXPERIMENTAL MODELING AND OPTIMIZATION OF CUTTING FORCE AND TOOL WEAR IN MICRO-TEXTURED TOOLS

5.1 Experimental Modeling Methodology

In this research, we investigated the influence of micro-grooved texture design on the cutting tool rake face for application of turning titanium alloy and steel alloy. In the experiments conducted, cutting forces and tool wear were measured.

Further investigations have been conducted on the effects of micro-grooved tool design upon cutting forces, tool temperature, tool stress and tool wear rate distributions, and variable friction coefficients. We proposed cutting of alloy steel 4340 with tungsten carbide tool having the texture with different spacing and width parameters. We have measured cutting forces, volumetric wear rate, and amount of material smearing into grooves.

The methodology involves machining alloy steel 4340 thin webs on rigid CNC machines with the specially designed textured tool; then measuring cutting forces using Kistler Type 9121 force dynamometer and Kistler Type 9121 turret adapter mounted on the CNC turret disk. Next, cutting tools were inspected under the metallurgical grade digit optical microscopy to measure the length of severe wear, sliding wear, and smearing wear regions.

Furthermore, areal surface height maps have been obtained from rake faces of micro-grooved tool inserts by using focus variation microscopy (FVM) system (Alicona InFocus G4 XL200) from which we acquired better information about volumetric smearing and volumetric wear. The last step of this methodology involves finding the analytical relationships between cutting forces, smearing and sliding wear and micro-texture parameters such as width, spacing, depth, the

location from the cutting edge, etc. with multivariate regression analysis. This experimental modeling methodology is summarized in Fig. 5.1.

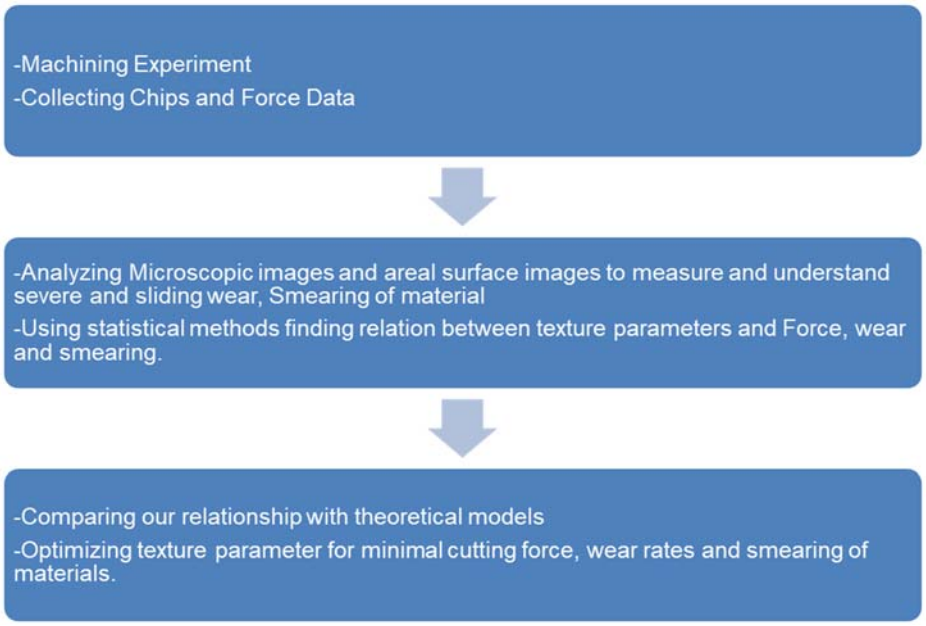

Figure 5.1 The methodology for experimental modeling and optimization of micro-texture parameters.

5.2 Experimental Force and Tool Wear Modeling

In our experiment for orthogonal cutting we would like to have a model which can predict the wear, smearing, cutting forces with fair accuracy. Some parameters of our experiments are variables, and some are constant. Constant parameters are such as axial depth of cut, removed material amount, rake angle, clearance angles, etc. will not affect our model. Other parameters which are independent variables such as the width of the groove (w), spacing of the groove (s), depth of the groove (d), cutting speed (v_c), feed rate (f) are considered in the regression model. The output parameters in this model are severe wear, sliding wear, smearing wear, thrust and cutting forces. We have multiple variables, so we have used a multivariate regression equation.

$$\hat{y}_i = \beta_0 + \beta_1(x_1) + \beta_2(x_2) + \beta_{11}({x_1}^2) + \beta_{22}({x_2}^2) + \beta_{12}(x_1 x_2) + \cdots \varepsilon_i \quad (5.1)$$

where x_1, x_2,…x_n are independent variables, and y_1, y_2, … y_n are dependent variables or responses, β_0 is the regression intercept, β_1, β_2… β_n are regression slopes, β_{11}, β_{22}, β_{12}… β_{mn} are model estimators for higher order terms as well as interaction terms, and $\varepsilon_i \sim$ N (0, σ^2) is a residual error (Montgomery 2009). For simplicity, we have only considered till second order polynomial terms and omit some interaction terms which has very negligible correlation values with our dependent variable. After that our x_i we choose were micro-texture groove width (*w*), spacing of groove (*s*), depth of groove (*d*), cutting speed (v_c), feed rate (*f*), distance from the cutting edge (*t), squared* cutting speed $(v_c)^2$, squared feed rate $(f)^2$, and interaction term of cutting speed and feed rate (v_c)* (*f*). Solving this would give us values of estimates of β_0, β_1, β_2…, β_n, β_{11}, β_{22}, β_{12}…, β_{mn} that will help us to understand the effect of the micro-texture parameters on the measured forces and tool wear. First, we started with considering the whole model as linear and using those predictors of beta we tried to minimize the standard error with GRG non-linear function in Excel. Using the knowledge, we can later optimize them to get minimum forces and minimum wear on the micro-texture tool. Force regression models are obtained for the thrust force $y_1 = F_t$, and the cutting force $y_2 = F_c$ where independent variables are $x_1 = v_c$, $x_2 = f$, $x_3 = w$, $x_4 = s$, $x_5 = d$, and $x_6 = t$ and the model predictors are as given in Table 5.1. For both models, adjusted R-squared was near 90% and then with the least square method, we further improved from there by a small margin.

Table 5.1 Experimental force model predictors.

	F_t [N/mm]	F_c [N/mm]
β_0	-1437.0734	-1764.1038
β_1	5.2858	10.4233
β_2	8288.1179	16796.3760
β_{11}	-0.0426	-0.0901
β_{22}	-27638.0929	-62322.1231
β_{12}	26.2359	54.4099
β_3	1.2919	0.6631
β_4	-0.7095	-0.1843
β_5	2.2702	4.0707
β_6	7.7461	5.0740
Std. error	37.1573	43.8413

Experimental wear regression models are for the severe wear length $y_1 = l_{severe}$, the sliding wear length $y_2 = l_{sliding}$, the smearing wear length $y_3 = l_{smearing}$, and the total wear length $y_3 = l_{total}$ where independent variables are $x_1 = v_c$, $x_2 = f, x_3 = w, x_4 = \mathrm{s}, x_5 = d$,and $x_6 = t$ and the model predictors are as given in Table 5.2. For all the wear models adjusted R-squared was nearly 97% so we did not apply least square method and just took linear regression estimates as our final estimates.

Table 5.2 Experimental wear model predictors.

	l_{severe} [µm]	$l_{sliding}$ [µm]	$l_{smearing}$ [µm]	l_{total} [µm]
β_0	-0.253682	0.003799	-0.028065	-0.249882
β_1	-0.001462	0.000290	0.003621	-0.001171
β_2	3.864928	1.323157	0.678685	5.188085
β_{11}	-0.000002	-0.000005	-0.000026	-0.000007
β_{22}	-14.661594	-3.501417	2.240181	-18.163011
β_{12}	0.008303	-0.001574	-0.010243	0.006729
β_3	-0.000518	0.000213	-0.000038	-0.000305
β_4	0.000186	-0.000024	0.000035	0.000162
β_5	-0.000205	0.000259	0.001924	0.000054
β_6	0.002877	0.000157	-0.000059	0.003034
Std. error	0.00825	0.003799	0.000205	0.008571

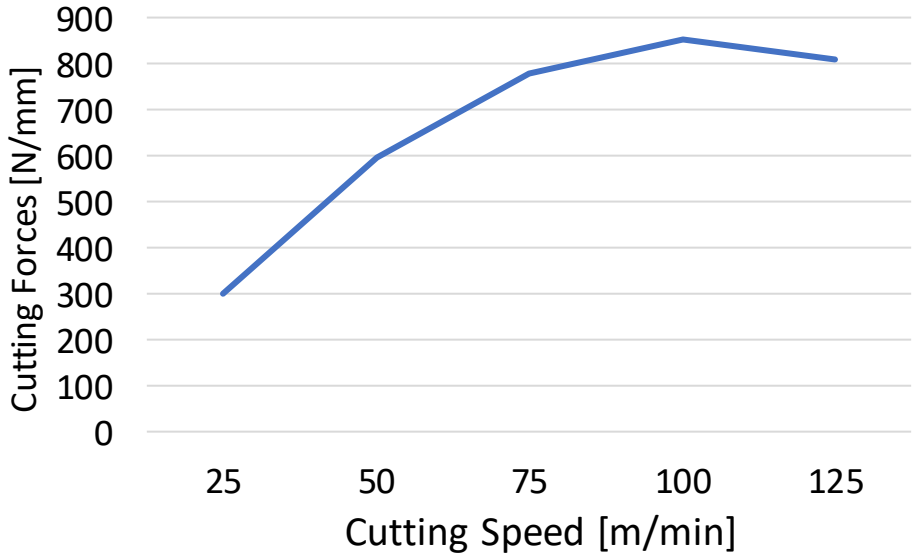

Figure 5.2 The effect of cutting speed on the cutting forces overall.

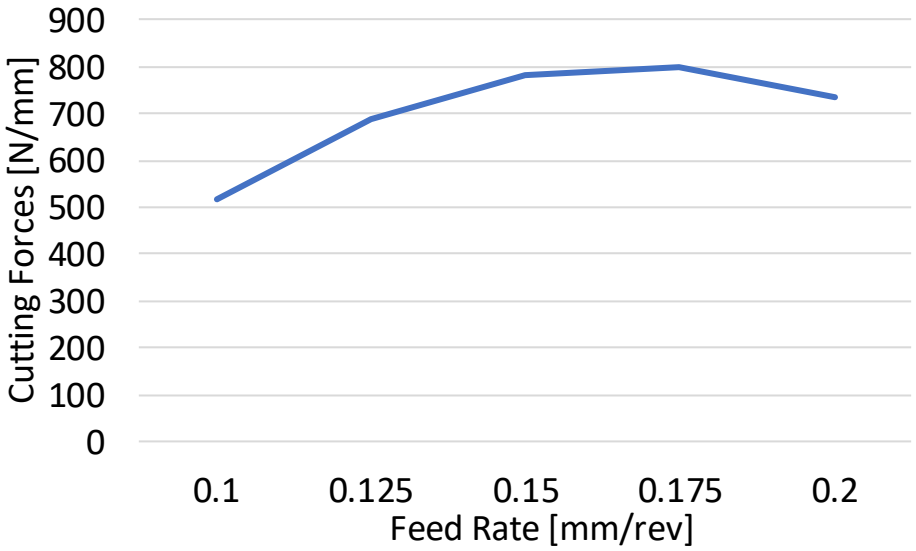

Figure 5.3 The effect of feed rate on the cutting forces.

5.3 Optimization of Micro-textured Cutting Parameters for Minimizing Cutting Force and Minimizing Tool Wear

The technique utilized for optimization of micro-texture parameters is a multi-objective genetic algorithm (MOGA) (Deb et al., 2002). MOPSO has been utilized extensively in multi-objective manufacturing optimization problems. The optimization problem deals with minimizing cutting force and minimizing wear hence improving tool life. For this optimization problem, we utilized the cutting force and wear regression models (Eqs. 5.2 and 5.3). Cutting force experimental model was utilized to define the first objective function as given below.

$$\hat{F}_c = -1764.103800 + 10.423300\,(v_c) + 16796.376000(f) - 0.090100({v_c}^2) - 62322.123100(f^2) + 54.409900(v_c * f) + 0.663100(w) - 0.184300(s) + 4.070700(d) + 5.074000_6(t) + \varepsilon_{Fc} \quad (5.2)$$

Measured length of wear in the experimental model was utilized as the second objective function as given below.

$$\hat{l}_{severe\ wear} = -0.253682 - 0.001462\ (v_c) + 3.864928(f) - 0.000002({v_c}^2) - 14.661594(f^2) + 0.008303(v_c * f) - 0.000518(w) + 0.000186(s) - 0.000205(\mathrm{d}) + 0.002877(t) + \varepsilon_{l\_severe\_wear} \quad (5.3)$$

$$\hat{l}_{smearing\ wear} = -1764.103800 + 10.423300(v_c) + 16796.376000(f) - 0.090100({v_c}^2) - 62322.123100(f^2) + 54.409900(v_c * f) + 0.663100(w) - 0.184300(s) + 4.070700(d) + 5.074000(t) + \varepsilon_{l\_smearing\_wear} \quad (5.4)$$

We have done this for the main two types of wear and cutting force only. Severe wear and sliding wear were increasing and decreasing in the same condition. So, we only took severe wear as our objective function. Severe wear and smearing wear are important and reduce the life of the tool very much. The objective function becomes as given in Eq. (5.5) in which l_{wear} will be taken from Eq. (5.3) and Eq. (5.4) for severe wear as $l_{severe\ wear}$ and smearing wear as $l_{smearing\ wear}$ respectively;

$$Minimize\ \{F_c(v_c, f, w, s, d, t)\ , l_{wear}(v_c, f, w, s, d, t)\ \} \quad (5.5)$$

The lower bound and upper bound for decision variables for this problem are given below.

0.1 mm/rev ≤ f ≤ 0.2 mm/rev

25 m/min ≤ v_c ≤ 125 m/min

50 μm ≤ w ≤ 100 μm

50 μm ≤ s ≤ 200 μm

100 ≤ t ≤ 150 μm.

Our first objective is to reduce cutting forces. Thrust and cutting forces have estimators similar in nature so we have optimized the microtextured parameters

for cutting forces only. The second objective is to reduce the tool wear and hence improve surface roughness as well as tool life cycle. Cutting forces and wear prediction models have predictors which are opposite in nature. We have used the Pareto frontier of non-dominating solutions to find out best combinations and from which we can choose the parameters based on our optimization strategy. For example, if the strategy is to have low cutting forces then we can select some decision variable combinations which will yield to lower cutting forces but at the cost of high tool wear. On the contrary, if the strategy is to have the lowest tool wear that set of decision variables may result in higher cutting forces.

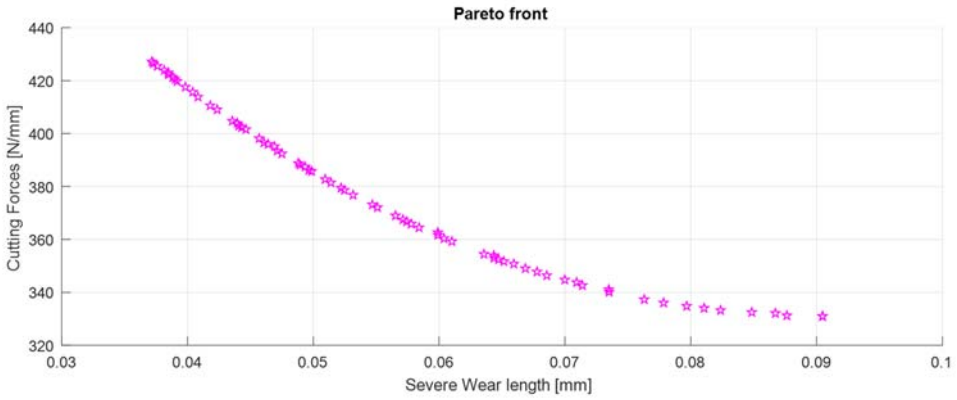

Figure 5.4 The Pareto frontier of the objective function space indicating cutting force vs severe wear length.

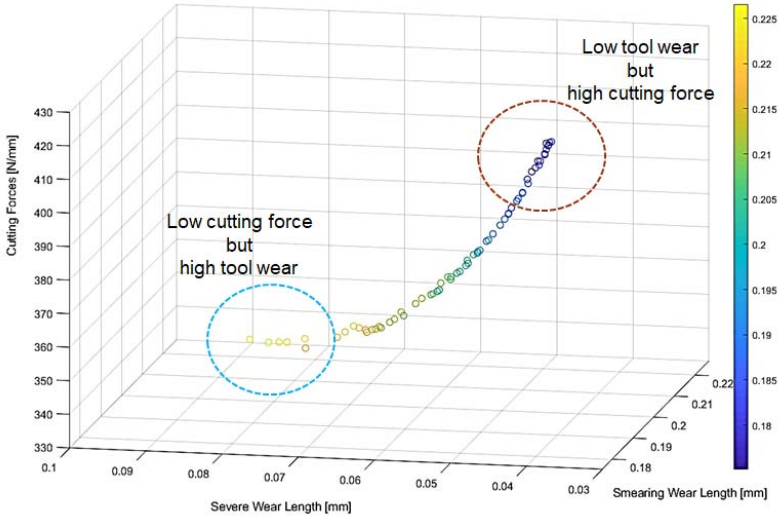

Figure 5.5 Objective function space (minimizing cutting forces and tool wear).

Table 5.3 The optimum solution set obtained from the MOPSO method.

v_c [m/min]	f [mm/rev]	w [μm]	s [μm]	d [μm]	t [mm]	l_{severe} [mm]	F_c [N/mm]	l_{smearing} [mm]
57.83	0.135	73.61	156.09	19.68	0.127	0.090	330.953	0.227
56.78	0.136	72.75	147.78	19.11	0.122	0.089	331.177	0.228
54.77	0.134	73.19	145.34	17.91	0.131	0.085	331.835	0.224
53.93	0.135	73.86	155.53	19.44	0.121	0.084	332.342	0.224
52.45	0.136	71.45	142.90	17.90	0.129	0.081	333.660	0.224
51.82	0.136	72.85	144.67	19.04	0.131	0.080	334.275	0.223
51.34	0.138	73.32	145.57	18.51	0.131	0.080	335.572	0.226
50.75	0.137	73.87	143.62	19.95	0.127	0.079	335.722	0.223
50.24	0.137	74.01	142.90	19.86	0.128	0.078	336.382	0.223
50.13	0.137	73.88	151.60	19.62	0.129	0.078	336.766	0.224
49.20	0.135	73.74	145.19	19.28	0.124	0.076	337.690	0.219
48.63	0.135	73.10	145.68	18.87	0.124	0.075	338.602	0.218
47.99	0.136	73.43	137.76	18.13	0.128	0.074	339.832	0.220
47.89	0.134	71.07	144.35	18.80	0.130	0.074	339.887	0.217
47.13	0.136	73.46	155.35	19.60	0.127	0.073	341.456	0.219
45.73	0.133	73.92	138.97	19.16	0.123	0.070	344.338	0.213
44.18	0.136	72.62	129.03	18.26	0.140	0.068	347.850	0.215
42.36	0.134	74.35	145.35	19.77	0.130	0.065	352.602	0.210
41.96	0.134	72.54	156.64	19.38	0.132	0.064	353.691	0.210
41.74	0.132	72.14	134.12	19.28	0.128	0.063	354.624	0.207
41.51	0.133	72.25	136.64	19.02	0.132	0.063	355.194	0.207
41.04	0.135	70.79	136.48	18.46	0.128	0.062	356.393	0.209
40.34	0.135	72.02	141.02	18.47	0.127	0.061	358.585	0.209
40.04	0.135	72.85	145.75	19.34	0.127	0.061	359.538	0.208
39.71	0.136	72.60	144.67	19.66	0.128	0.060	360.654	0.208
39.38	0.135	72.72	136.61	19.29	0.127	0.060	361.664	0.207
39.09	0.133	71.71	139.23	19.36	0.130	0.059	362.749	0.204
38.74	0.136	72.78	141.61	18.52	0.127	0.059	363.925	0.207
38.64	0.136	73.17	141.68	18.59	0.128	0.059	364.216	0.206
38.40	0.137	72.28	138.53	19.21	0.130	0.058	365.202	0.207
37.89	0.136	73.17	138.82	18.70	0.128	0.057	366.888	0.205
37.62	0.138	72.59	137.09	18.84	0.127	0.057	368.601	0.208
37.06	0.134	73.08	142.50	19.90	0.129	0.056	369.887	0.202
36.71	0.137	73.78	145.38	19.65	0.128	0.056	371.412	0.204
36.70	0.133	71.73	133.33	19.38	0.130	0.055	371.433	0.200
36.34	0.133	70.37	135.87	18.32	0.131	0.055	372.863	0.199
35.89	0.135	73.32	141.13	19.36	0.128	0.054	374.399	0.201

v_c [m/min]	f [mm/rev]	w [μm]	s [μm]	d [μm]	t [mm]	l_{severe} [mm]	F_c [N/mm]	l_{smearing} [mm]
34.57	0.135	73.16	140.92	18.66	0.128	0.052	379.755	0.198
34.30	0.136	72.29	140.73	17.99	0.127	0.052	380.941	0.199
34.12	0.136	71.91	138.88	18.91	0.130	0.051	381.746	0.199
33.35	0.134	73.08	154.04	18.71	0.132	0.050	385.078	0.195
33.18	0.133	71.34	140.54	18.09	0.130	0.050	385.872	0.194
32.77	0.134	73.14	154.31	19.06	0.132	0.049	387.677	0.193
32.71	0.133	70.95	140.82	18.52	0.128	0.049	388.111	0.192
32.47	0.136	71.20	136.03	17.17	0.139	0.049	388.972	0.195
32.21	0.131	72.07	136.61	18.41	0.134	0.048	390.927	0.189
32.05	0.133	72.82	153.24	19.65	0.130	0.048	391.098	0.191
31.72	0.133	72.52	133.18	17.53	0.138	0.047	392.639	0.191
31.51	0.135	72.57	130.69	18.80	0.129	0.047	393.455	0.192
31.27	0.135	72.96	137.47	18.44	0.130	0.047	394.597	0.192
31.17	0.135	71.63	143.65	18.26	0.135	0.047	395.077	0.192
30.99	0.133	73.78	131.12	17.60	0.135	0.046	396.155	0.189
30.54	0.136	71.63	137.09	17.39	0.131	0.046	398.184	0.192
30.07	0.135	72.88	142.23	18.38	0.130	0.045	400.433	0.189
29.82	0.134	72.45	150.45	18.91	0.132	0.044	401.786	0.188
29.23	0.133	72.44	137.29	19.22	0.127	0.043	404.844	0.186
28.90	0.137	72.80	140.44	18.62	0.127	0.043	406.831	0.190
28.75	0.136	72.80	145.40	18.48	0.129	0.043	407.334	0.188
27.97	0.135	73.85	148.95	19.51	0.129	0.042	411.332	0.185
27.74	0.134	72.33	136.60	18.45	0.131	0.041	412.683	0.183
27.30	0.136	71.86	138.13	18.35	0.134	0.041	415.046	0.185
26.90	0.136	70.96	132.66	19.01	0.138	0.040	417.299	0.184
26.76	0.132	71.32	131.68	17.85	0.130	0.040	418.653	0.178
26.40	0.134	72.16	148.58	18.42	0.130	0.039	420.035	0.181
26.02	0.134	70.66	136.91	17.74	0.129	0.038	422.300	0.179
25.88	0.135	72.95	135.42	18.37	0.134	0.038	423.035	0.181
25.60	0.132	71.93	136.30	18.02	0.132	0.038	424.995	0.177
25.31	0.135	71.18	129.04	18.36	0.140	0.037	426.319	0.180
25.02	0.134	70.66	135.91	17.74	0.129	0.037	428.125	0.177
25.02	0.134	70.66	137.91	17.74	0.129	0.037	428.125	0.177

CHAPTER 6

CONCLUSIONS AND FUTURE SCOPE

In this research, we investigated the effect of various micro-textured insert designs on the cutting forces and tool wear with experiments in machining titanium alloy Ti-6Al-4V and alloy steel 4340. It was found that micro-texture parameters affect cutting forces and tool wear from the cutting forces measured by force dynamometers and the surface topography of the micro-textured tool surfaces inspected using optical microscopy. Focus variation techniques also proved that smearing of material is taking place which demonstrates that micro-texture on the rake face engages during the cutting action. Micro-texture parameters; groove depth, width, and spacing, are found to be influential on the amount of material smearing into grooves and adhering on the tool surface while reducing thrust forces due to lower contact. Multi-objective optimization studies were conducted to find cutting conditions and micro-groove parameters in machining steel alloy 4340 that minimizes cutting forces and wear. Therefore, the micro-texture design on the tool surfaces can be optimized to obtain lowered cutting forces, improved tool wear, and minimal material adherence. The following specific conclusion has been made from the study in this thesis.

- Force prediction and wear prediction models were able to explain the effect of feed rate on the cutting forces and tool wear with the micro-grooved tool with very fair accuracy. The cutting forces increased rapidly between low to medium cutting speed range while for medium to high cutting speed conditions, it increased at a lower rate. Severe tool wear length was found to be reduced with an increase in cutting speed gradually. Increase in feed rate also indicated an increase in severe tool wear. Smearing wear was found to be dropping significantly with increase in cutting speed. But, with increasing feed rate, material smearing into micro-grooves was seen developing rapidly.

- Cutting forces were observed to be reduced when micro-groove width was reduced and micro-groove spacing was increased. Increased micro-groove

depth allowed more material to deform inside micro-grooves and added more friction and hence more cutting forces.

- For the identification of the effect of micro-groove optimum width and depth values that may minimize cutting forces, the MOPSO method was used to obtain optimal solution sets and among these preferred decision variables can be selected.

- When the chip load was covering a portion of the micro-textured area, cutting forces seemed to be reduced even when increasing the feed rate. This phenomenon explains that normal stresses on the tool rake surface were reduced due to micro-textured geometry reducing friction of coefficient.

- The average friction coefficient of cutting operation was found lower than regular value, even without use of lubricants or coolants.

The future scope of study about this field is limitless. The micro-textures applied to cutting tools proved to be helpful in reducing cutting forces and tool wear. If using micro-grooves as texture, for any type of geometry of insert, groves perpendicular to the cutting and in the direction of chip flow will be the best choice because it will not generate any type of extra resistant to the machined chips. More variety of the micro-textures such as sine-wave, rounded wall edges, and other shape of texture geometry can be tested to find more effective micro-texture patterns. Coating might not be feasible with micro-texture. Although, with good strategy to apply coating in limited selective area can open new direction. Furthermore, micro-textures will enable a better use of solid lubricants (e.g. molybdenum disulfide (MoS_2, hexagonal boron nitride (h-BN)), minimal quantity lubricants, near- dry cutting or cryogenic cutting methods which will help achieve environmentally sustainable machining practices.

REFERENCES

Arrazola, P.J., Özel, T., Umbrello, D., Davies, M., Jawahir, I.S. (2013) Recent Advances in Modelling of Metal Machining Processes. CIRP Annals-Manufacturing Technology 62(2): 695–718.

Arslan, A., Masjuki, H.H., Kalam, M.A., Varman, M., Mufti, R.A, Mosarof, M.H, Khuong, L.S., Quazi, M.M. (2016) Surface Texture Manufacturing Techniques and Tribological Effect of Surface. Critical Reviews in Solid State and Materials Sciences 1: 1–35.

Bouzakis, K.D., Michailidis, N., Skordaris, G., Bouzakis, E., Biermann, D., M'Saoubi, R. (2012) Cutting with coated tools: coating technologies, characterization methods and performance optimization. CIRP Annals of Manufacturing Technology 6(2): 703-7012.

Chang, W., Sun, J., Luo, X., Chris, J.M. (2011) Investigation of microstructured milling tool for deferring tool wear. Wear 271(9-10): 2433–2437.

Deb, K., Pratap, A., Agarwal, S., Meyarivan, T. (2002) A fast and elitist multiobjectivegenetic algorithm: NSGA-II, IEEE Transactions on Evolutionary Computation 6: 182–197.

Enomoto, T., Sugihara, T. (2010) Improving anti-adhesive properties of cutting tool surfaces by nano-/micro-textures. CIRP Annals - Manufacturing Technology 59(1): 597–600.

Enomoto, T., Sugihara, T., Yukinaga, S., Hirose, K., Satake, U. (2012) Highly wear-resistant cutting tools with textured surfaces in steel cutting. CIRP Annals - Manufacturing Technology 61(1): 571–574.

Enomoto, T., Watanabe, T., Aoki, Y., Ohtake, N. (2007) Development of a Cutting Tool with Micro Structured Surface. Transaction of the Mechanical Society of Mechanical Engineers Series C73(729): 1560–1565.

Enomoto, T., Watanabe, T., Aoki, Y., Ohtake, N. (2006) Development of a Cutting Tool with Micro Engineering Surface. Proceedings of Spring Conference of the Japan Society for Precision Engineering: 281–282.

Evans C.J., Bryan J. (1999) “Structured”, “Textured” or “Engineered” Surfaces. CIRP Annals - Manufacturing Technology 48(2): 541–556.

Filipovic, A., Stephenson, D.A. (2006) Minimum Quantity Lubrication (MQL) Applications in Automotive Powertrain Machining. Machining Science and Technology 10(1): 3–22.

Fratila, D. (2010) Macro-Level Environmental Comparison of Near-Dry Machining and Flood Machining. Journal of Cleaner Production 18(10–11): 1031–1039.

Haapala, K.R., Zhao, F., Camelio, J., Sutherland, J.W., Skerlos, S.J., Dornfeld, D.A., Jawahir, I.S., Clarens, A.F., Rickli, J.L. (2013) A Review of Engineering Research in Sustainable Manufacturing. Journal of Manufacturing Science and Engineering 135(4), 1-15.

Helu, M., Behmann, B., Meier, H., Dornfeld, D., Lanza, G., Schulze, V. (2012) Impact of green machining strategies on achieved surface quality. CIRP Annals - Manufacturing Technology 61(1): 55-58.

Jawahir, I.S., Attia, H., Biermann, D., Duflou, J., Klocke, F., Meyer, D., Newman, S.T., Pusavec, F., Putz, M., Rech, J., Schulze, V., Umbrello, D. (2016) Cryogenic manufacturing processes. CIRP Annals - Manufacturing Technology 65(2): 713-736.

Jianxin, D., Wenlong, S., Hui, Z. (2009) Design, fabrication and properties of a self-lubricated tool in dry cutting. International Journal of Machine Tools and Manufacture 49 (1): 66–72.

Jianxin, D., Ze, W., Yunsong, L., Ting, Q., Jie, C. (2012) Performance of carbide tools with textured rake-face filled with solid lubricants in dry cutting processes. International Journal of Refractory Metals and Hard Materials 30 (1): 164–172.

Kawasegi, N., Sugimori, H., Morimoto, H., Morita, N., Hori, I. (2009) Development of cutting tools with microscale and nanoscale textures to improve frictional behavior. Precision Engineering 33(3): 248–254.

Kawasegi, N., Morimoto, H., Morita, N., Hori, I. (2010a) Development of small-diameter drill with micro/nanometer-scale textures. The Japan Society of Mechanical Engineers.

Kawasegi, N.; Sugimori, H., Morimoto, H., Morita, N., Hori, I. (2010b) Drilling Aluminum Allow Using Small-Diameter Drills with Micro/Nanometer-Scale Textures. The Japan Society of Mechanical Engineers 76 (762): 446–452.

Klocke, F., Eisenblätter, G. (1997) Dry cutting. CIRP Annals- Manufacturing Technology 46 (2): 519-526.

Koshy, P., Tovey, J. (2011) Performance of electrical discharge textured cutting tools. CIRP Annals - Manufacturing Technology 60(1): 153–196.

Lei, S., Devarajan, S., Chang, Z. (2009) A study of micropool lubricated cutting tool in machining of mild steel. Journal of Materials Processing Technology 209 (3): 1612–1620.

Manikandan, N., Kumanan, S., Sathiyanarayanan, C. (2016) Multiple performance optimization of electrochemical drilling of Inconel 625 using Taguchi based Grey Relational Analysis. Engineering Science and Technology, An International Journal. 20(2): 662-671.

Montgomery, D.C. (2009) Introduction to Statistical Quality Control. John Wiley & Sons, Inc. Hoboken, New Jersey.

Nakano, M.., Korenaga, A., Korenaga, A., Miyake, K., Murakami, T., Ando, Y. (2007) Applying Micro-Texture to Cast Iron Surfaces to Reduce the Friction Coefficient Under Lubricated Conditions. Tribology Letters 28 (2): 131–137.

Pou, P., Riveiro, A., del Val J., Comesaña, R., Penide, J., Arias-González, F., Soto R., Lusquiños, F., Pou, J. (2017) Laser surface texturing of titanium for bioengineering applications. Procedia Manufacturing 13: 694-701.

Ramesha, A., Akrama, W., Mishra, S., Cannon, A.H., Polycarpou, A.A., King, W.P. (2013) Friction characteristics of micro textured surfaces under mixed and hydrodynamic lubrication. Tribology International 57: 170–176.

Sharma, V., Pandey, P.M. (2016) Recent advances in turning with textured cutting tools: A review, Journal of Cleaner Production 137: 701-715.

Shin, M., Senoaji, A.H., Kwon, S., Chung, W., Kwon, S., Park, J., Kim J., Choi, W. (2015) Characteristic of Friction on Texturing Bearing Steel with Ultrasonic Hole Machine Journal of Korean Society of Tribology, Lubrication Engineering 31(1): 21-27.

Sugihara, T., Enomoto, T. (2009) Development of a cutting tool with a nano/micro-textured surface-Improvement of anti-adhesive effect by considering the texture patterns. Precision Engineering 33 (4): 425–429.

Sugihara, T., Enomoto, T. (2012) Improving anti-adhesion in aluminium alloy cutting by micro stripe texture. Precision Engineering 36 (2): 229–237.

Sugihara, T., Enomoto, T. (2013) Crater and flank wear resistance of cutting tools having micro textured surfaces. Precision Engineering 37 (4): 888–896.

Wei, Tang, Yuankai, Z., Hua, Z., Haifeng, Y. (2013) The effect of surface texturing on reducing the friction and wear of steel under lubricated sliding contact. Applied Surface Science 273: 199–204.

Sugihara, T., Enomoto, T. (2017) Performance of cutting tools with dimple textured surfaces: A comparative study of different texture patterns. Precision Engineering 49: 52-60.

Wang, Y.Q., Wu, G., Han, Q., Fang, L., Ge, S.R. (2009) Tribological properties of surface dimple-textured by pellet-pressing. Procedia Earth and Planetary Science 1: 1513–1518.

Weinert, K., Inasaki, I., Sutherland, J.W., Wakabayashi, T. (2004) Dry machining and minimum quantity lubrication, CIRP Annals - Manufacturing Technology 53(2): 511-537.

Xie, J., Luo, M.J., He J.L., Liu X.R., and Tan T.W. (2012) Micro-grinding of micro-groove array on tool rake surface for dry cutting of titanium alloy. International Journal of Precision Engineering and Manufacturing 13(10): 1845–1852.

Yang, Y., Su, Y., Li, L., He, N., Zhao, W. (2015) Performance of cemented carbide tools with microgrooves in Ti-6Al-4V titanium alloy cutting. International Journal Advanced Manufacturing Technology 76(9): 1731–1738.

Zorev, N.N. (1963) Inter-relationship between shear processes occurring along tool face and shear plane in metal cutting. International Research in Production Engineering ASME: 42-49.